Article

SOURCE DATA | TRANSPARENT PROCESS | OPEN ACCESS

EMBO reports

LRH-1/NR5A2 interacts with the glucocorticoid receptor to regulate glucocorticoid resistance

Svenja Michalek[1,2], Thomas Goj[1], Anna Pia Plazzo[1], Blerim Marovca[3], Beat Bornhauser[3] & Thomas Brunner[1,2,*]

Abstract

Nuclear receptors are transcription factors with important functions in a variety of physiological and pathological processes. Targeting glucocorticoid receptor (GR) activity using glucocorticoids is a cornerstone in the treatment of patients with T cell acute lymphoblastic leukemia (T-ALL), and resistance to GC-induced cell death is associated with poor outcome and a high risk for relapse. Next to ligand-binding, heterodimerization with other transcription factors presents an important mechanism for the regulation of GR activity. Here, we describe a GC-induced direct association of the Liver Receptor Homolog-1 (LRH-1) with the GR in the nucleus, which results in reciprocal inhibition of transcriptional activity. Pharmacological and molecular interference with LRH-1 impairs proliferation and survival in T-ALL and causes a profound sensitization to GC-induced cell death, even in GC-resistant T-ALL. Our data illustrate that direct interaction between GR and LRH-1 critically regulates glucocorticoid sensitivity in T-ALL opening up new perspectives for developing innovative therapeutic approaches to treat GC-resistant T-ALL.

Keywords apoptosis; glucocorticoid receptor; liver receptor homolog-1 (LRH-1); NR5A2; T cell acute lymphoblastic leukemia

Subject Categories Cancer; Chromatin, Transcription, & Genomics; Signal Transduction

DOI 10.15252/embr.202154195 | Received 20 October 2021 | Revised 9 June 2022 | Accepted 14 June 2022 | Published online 8 July 2022

EMBO Reports (2022) 23: e54195

Introduction

Liver Receptor Homolog-1 (LRH-1/NR5A2) is a transcription factor of the nuclear receptor (NR) superfamily that is primarily expressed in epithelial tissues of endodermal origin, including the liver, pancreas, gastro-intestinal tract and reproductive organs (Bookout *et al*, 2006). It is considered an orphan NR as, contrary to most NRs, no endogenous LRH-1 ligands have been identified so far. While LRH-1 has a constant nuclear localization and maintains a transcriptionally active conformation (Sablin *et al*, 2003), its activity is further regulated by co-activators and co-repressors, post-translational modifications as well as substances interacting with the ligand-binding pocket (Stein & Schoonjans, 2015). Regulating the transcription of a plethora of target genes, LRH-1 is critically involved in a wide variety of biological processes. It is vital during embryonic development and further regulates different metabolic pathways in the adult organism, including cholesterol and bile acid homeostasis (Pare *et al*, 2004), as well as glucose-sensing and processing (Oosterveer *et al*, 2012). In addition, LRH-1 was shown to be a critical regulator of cellular proliferation (Botrugno *et al*, 2004), stemness (Heng *et al*, 2010), stress response pathways (Mamrosh *et al*, 2014) as well as local steroidogenesis, e.g. glucocorticoid (GC) synthesis in the intestinal epithelium, as reviewed by Merk *et al* (2021). As deregulation of these processes results in a selective proliferative and survival advantage and is commonly associated with cancer, LRH-1 has been proposed to be a potential oncogene (Nadolny & Dong, 2015). In recent years, LRH-1, thus, gained increasing attention in the field of cancer research, and its overexpression and/or deregulation is clearly linked to different types of solid cancer. Several independent studies demonstrated an implication of LRH-1 in the development and progression of human pancreatic (Chen *et al*, 2018), colon (Wu *et al*, 2018), breast (Pang *et al*, 2017), liver (Xiao *et al*, 2018), prostate (Porter *et al*, 2019) and gastric cancer (Liu *et al*, 2019).

Whereas the function of LRH-1 in epithelial tissues and associated tumors is rather well explored, until today, very little is known about its role in the hematopoietic system and associated malignancies. Only recently, we were able to demonstrate that LRH-1 has important regulatory functions in different immune cells, even though its expression levels in these cell types are comparably low. LRH-1 directly regulates the transcription of Fas (CD95) ligand in cytotoxic T cells (Schwaderer *et al*, 2017) and controls the production of pro-inflammatory cytokines in macrophages (Lefevre *et al*, 2015; Schwaderer *et al*, 2020). Most importantly, however, LRH-1 is a critical regulator of T cell proliferation and, thus, T cell-mediated immune responses by regulating the transcription of cell cycle regulators, including c-Myc, and cyclin D1 and E1. In addition, LRH-1 seems to have important anti-apoptotic functions as its

1 Department of Biology, Biochemical Pharmacology, University of Konstanz, Konstanz, Germany
2 Konstanz Research School Chemical Biology KORS-CB, University of Konstanz, Konstanz, Germany
3 Division of Oncology and Children's Research Centre, University Children's Hospital Zurich, Zurich, Switzerland
*Corresponding author. Tel: +49 7531 88 5371; E-mail: thomas.brunner@uni-konstanz.de

deletion results in elevated basal as well as mitogen-induced cell death of T cells (Seitz *et al*, 2019). Along these lines, acute deletion of LRH-1 in intestinal epithelial cells similarly results in extensive cell death induction (Bayrer *et al*, 2018).

In contrast to these mitogenic and pro-survival functions of LRH-1, the glucocorticoid receptor (GR/NR3C1) is well known for its anti-proliferative as well as cell death-inducing activities in T cells (Almawi & Melemedjian, 2002; Herold *et al*, 2006). Like LRH-1, the GR is a transcription factor of the NR superfamily (Mangelsdorf *et al*, 1995). Its activity is, however, predominantly regulated by ligand-binding, which results in its dissociation from chaperone complexes and translocation to the nucleus (Timmermans *et al*, 2019). There, the GR binds to the DNA as a homodimer at glucocorticoid responsive elements (GRE) to transactivate or repress target gene expression (Louw, 2019). Due to their anti-inflammatory and immune-suppressive effects, GCs are among the most important drugs to treat auto-immune and inflammatory diseases (Petrillo *et al*, 2017), but also hematological cancer, including T cell acute lymphoblastic leukemia (T-ALL; Inaba & Pui, 2010). This particularly aggressive form of blood cancer results from the malignant transformation and subsequent uncontrolled clonal expansion of immature T cell progenitors (Hefazi & Litzow, 2018). Accumulation of these leukemic T cell blasts in the bone marrow and other organs results in a decreased production as well as a harmful imbalance of healthy blood components, and consequently functional insufficiency of the hematopoietic system (Terwilliger & Abdul-Hay, 2017). For many years synthetic GCs, such as dexamethasone, are among the most essential and effective drugs in the treatment of T-ALL, inhibiting proliferation and inducing cell death of leukemic T cells. Many patients, however, exhibit a poor response to GC treatment, which limits the therapeutic effect of GCs (Olivas-Aguirre *et al*, 2021). Despite extensive research effort, the molecular basis of GC sensitivity and resistance remains only poorly understood, and different mechanisms and their combinations contribute to GC resistance observed in individual patients (Clarisse *et al*, 2020). Failure of leukemic cells to undergo GC-induced cell death is, however, often associated with the lack of GC-mediated GR auto-upregulation and induction of the pro-apoptotic BCL-2 homolog and BH3-only protein Bim (Riml *et al*, 2004; Jing *et al*, 2015).

Apart from ligand-binding, target gene regulation by NRs is mainly regulated by multiple protein–protein interactions. These interactions occur between NRs and designated adapter proteins, co-activators and repressors, but these also include the formation of homodimers as well as heterodimers with other transcription factors, including other NRs (Amoutzias *et al*, 2007; Weikum *et al*, 2018). Especially important regarding GC resistance are the physical interactions of ligand-bound GR with nuclear factor 'kappa-light-chain-enhancer' of activated B cells (NF-κB) or activator protein 1 (AP-1), which reciprocally inhibit their transcriptional activity (McKay & Cidlowski, 1998). GR interactions with NF-κB and AP-1 and associated suppression of pro-inflammatory factor expression are primarily responsible for the anti-inflammatory effects of GCs (Escoter-Torres *et al*, 2019). Vice versa, the mutual antagonism of GR and NF-κB, respectively, AP-1, has been proposed to contribute to GC resistances observed in different hematopoietic malignancies (de Bosscher *et al*, 2003). Furthermore, similar protein–protein interactions between the GR and the orphan NR nerve growth factor IB (NGFI-B/Nur77/NR4A1) result also in reciprocal transrepression (Martens *et al*, 2005). Interestingly, LRH-1 activity can likewise be repressed by its direct interaction with NF-κB (Huang *et al*, 2014), and the atypical NR and LRH-1 target small heterodimer partner (SHP/NR0B2; Ortlund *et al*, 2005).

Based on these findings, we hypothesized that GR and LRH-1 could possibly interact in a similar manner. Indeed, we here report a direct physical interaction of the GR with LRH-1 that mediates a reciprocal inhibition of both transcription factors. Confirming the role of LRH-1 in the proliferation of T cells as well as its oncogenic properties observed in different solid cancers, we further show that LRH-1 is a critical regulator of T-ALL cell proliferation and survival as LRH-1 inhibition or downregulation results in growth defects and apoptosis. Furthermore, we obtained evidence that the physical interaction and mutual antagonism of the GR and LRH-1 plays a role in pathophysiological GC resistance. Pharmacological inhibition as well as LRH-1 knockdown sensitized T-ALL cells for GC-induced apoptotic cell death. This sensitization seems to be mediated by an improved auto-upregulation of the GR and Bim induction in response to GCs. Importantly, synergistic cell death induction by combined treatment with dexamethasone and LRH-1 inhibitor was also observed in primary tumor cells from T-ALL patients *in vitro* and *in vivo* in a xenograft transplantation model.

Taken together, this study reports for the first time a physical interaction and a mutual antagonism between the GR and LRH-1 that plays a role in GC sensitivity. It further demonstrates a critical role of LRH-1 in leukemic T cells, which opens new perspectives in developing novel therapeutic strategies in the treatment of T-ALL.

Results

Co-localization and physical interaction of GR and LRH-1 in the presence of dexamethasone

It is a well-established fact that the transcriptional activity of NRs is not solely determined by ligand-binding or post-translational modifications but also by interactions with co-modulatory factors. These protein–protein interactions occur between NRs and certain accessory co-activators or -repressors, chaperones, DNA modifiers/readers, but also other transcription factors, and play a critical role in the transcriptional regulation of NRs. In order to investigate whether the physical interaction between GR and LRH-1 could contribute to their reciprocal regulation, we investigated their subcellular localization.

Whereas LRH-1 constantly exhibits nuclear localization, the GR is sequestered in the cytosol under steady state conditions. (Fig 1A, upper panel). Thus, co-localization of the GR and LRH-1, an essential prerequisite for their physical interaction, may only occur in the presence of natural or synthetic GCs, such as dexamethasone. Dexamethasone induced a rapid translocation of the GR to the nucleus, where it co-localized with LRH-1 (Fig 1A, lower panel). LRH-1 and myc/His-tagged GR (mh-GR) could be co-precipitated by His-tag pulldown when both proteins were overexpressed in the human embryonic kidney (HEK) 293T cells (Fig EV1A), providing the first evidence for their direct physical interaction. Due to an overexpression-induced spontaneous nuclear translocation of the GR, co-precipitation of LRH-1 from nuclear extracts could be observed also in untreated cells but was substantially enhanced upon dexamethasone stimulation. To circumvent the limitations of

co-precipitation to unequivocally detect direct protein–protein interactions (Elion, 2006) and to exclude the possibility that the GR and LRH-1 are not directly interacting parts of a large multi-protein complex, we next exploited bimolecular fluorescence complementation (BiFC). For that purpose, two eYFP (enhanced yellow fluorescent protein) fragments, referred to as YFP1 (residues 1–157) and YFP2 (residues 158–238), were fused to the N-terminus of LRH-1 (YFP1-LRH-1), respectively, C-terminus of GR (GR-YFP2) as schematically depicted in Fig 1B. Whereas the single split-YFP fusion proteins are not fluorescent (Fig EV1B and D), direct physical interaction of

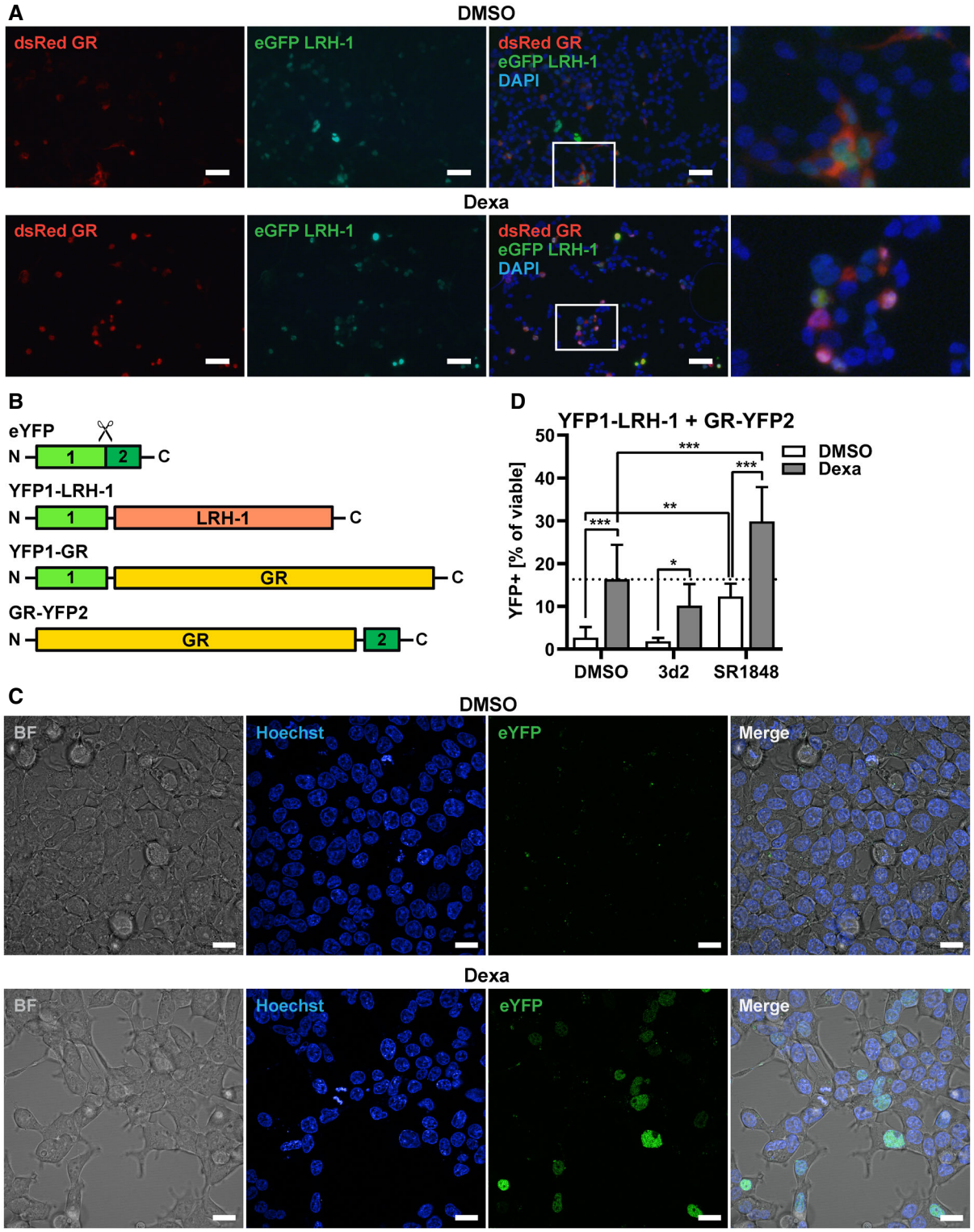

Figure 1.

Figure 1. Co-localization and physical interaction of GR and LRH-1 in the presence of dexamethasone.

A Fluorescence microscopy analysis of HEK 293T cells co-transfected with eGFP-tagged hLRH-1 (eGFP LRH-1) and dsRed-tagged hGR (dsRed GR) treated with dexamethasone (Dexa) or dimethyl sulfoxide (DMSO; solvent control). 4′,6-diamidino-2-phenylindole (DAPI; blue) was used for nuclear counterstain. Scale bar, 50 μm; 20x objective. Boxed areas are 4x magnified and shown at the right. Representative images of four biological replicates are shown.

B Schematic overview of the split eYFP protein and tagged LRH-1 and GR BiFC constructs. eYFP residues from 1–157 (YFP-1) are colored in light green and residues from 158–233 (YFP-2) are colored in dark green.

C Confocal fluorescence microscopy analysis of HEK 293H cells transiently transfected with YFP1-LRH-1 and GR-YFP2 for detection of BiFC formation (eYFP) in absence (DMSO) and presence of Dexa. Hoechst33342 was used for nuclear counterstain. Representative images of three biological replicates are shown and merged with the corresponding brightfield (BF) image. Scale bar: 20 μm; 40x objective.

D Flow cytometry-based quantification of BiFC in HEK 293H transiently co-transfected with YFP1-LRH-1 and GR-YFP2 and pre-treated for 6 h with 3d2 or SR1848, before stimulation with Dexa (2 h). BiFC positive (YFP+) cells are shown as a percentage (%) of viable cells. Dashed line indicates percentage of Dexa-driven BiFC positive cells. Data are shown as mean ± SD of nine (DMSO) and four (3d2/SR1848) biological replicates. Two-way ANOVA; *$P < 0.05$, **$P < 0.01$, ***$P < 0.001$.

YFP1-LRH-1 with GR-YFP2 should facilitate the reconstitution of native eYFP. As the intensity of BiFC is often low (< 10%) in comparison to the full length wild type protein (Kerppola, 2008), we first ensured that the reassembled eYFP emits sufficiently strong fluorescence upon excitation. Making use of the fact that the GR forms homodimers, we confirmed that a combination of the GR C-terminally tagged with the YFP1 fragment (YFP1-GR) and GR-YFP2 yields a profound BiFC signal that can not only be detected qualitatively by fluorescence microscopy (Fig EV1C) but also quantified by flow cytometry (Fig EV1D). Confirming the known GC-dependent subcellular localization of the GR (Nicolaides *et al*, 2000), YFP fluorescence was restricted to the cytosol in the absence and to the nucleus in the presence of dexamethasone (Fig EV1C). Simultaneous expression of YFP1-GR and GR-YFP2 resulted in approximately 40% YFP positive (YFP+) cells and was thus a suitable positive control for all following experiments (Fig EV1D).

As expected, hardly any BiFC was observed in unstimulated YFP1-LRH-1- and GR-YFP2-expressing HEK 293H cells (Fig 1C, upper panel). In contrast, dexamethasone-induced activation of the GR resulted in a clear induction of exclusively nuclear BiFC, as assessed by confocal fluorescence microscopy (Fig 1C, lower panel). Quantification of YFP+ cells via flow cytometry confirmed the significant induction of GR-LRH-1 BiFC upon dexamethasone stimulation (Fig 1D).

These results clearly demonstrate a novel direct physical interaction of the GR and LRH-1, which may have potential regulatory functions. We, thus, next investigated whether and how this GC-mediated interaction might be affected by two small molecule LRH-1 antagonists. As previously shown by Benod *et al* (2013), compound 3d2 specifically binds to and induces a conformational change of the LRH-1 ligand-binding domain that diminishes its interaction with co-regulatory proteins (Benod *et al*, 2013). The second, even more potent LRH-1 antagonist SR1848 induces its rapid translocation from the nucleus to the cytoplasm of cells (Corzo *et al*, 2015). Via different modes of action, both compounds hence not only inhibit LRH-1 activity but also alter its interaction with co-regulatory factors. Interestingly, we observed opposing effects of 3d2 and SR1848 on the GR-LRH-1 interaction as assessed by analysis of YFP1-LRH-1 and GR-YFP2 BiFC via fluorescence microscopy (Fig EV1E) and flow cytometry (Fig 1D). Showing no effect in the absence of GCs, 3d2 slightly reduced the dexamethasone-mediated increase in BiFC positive cells (Fig 1D). Contrary, SR1848-mediated nuclear export of LRH-1 did not only facilitate co-localization but also significant interaction with the GR in the cytoplasm of cells (Fig EV1E). Furthermore, SR1848 roughly doubled the amount of dexamethasone-induced YFP+ cells and, thus, unlike 3d2, strongly reinforces the GR-LRH-1 protein–protein interaction (Fig 1D).

In summary, these data provide evidence for a physical interaction of the GR and LRH-1 that is promoted by GC-induced co-localization of both NRs in the nucleus and that can be modulated by small molecule LRH-1 antagonists.

Reciprocal inhibition of the GR and LRH-1

We next determined whether the physical interaction of the GR and LRH-1 impacts the activity of one or both transcription factors. Therefore, HEK 293T cells were transfected with either a GC response element (GRE) or 5-fold LRH-1 response element (5xRE) luciferase reporter and were treated with dexamethasone and/or LRH-1 antagonists (3d2, SR1848) to assess the effects on GR and LRH-1 transcriptional activity, respectively. First, validating the functionality and suitability of these reporter assays, dexamethasone treatment induced the GR promoter activity that could be significantly enhanced by GR overexpression, and that was inhibited upon pre-treatment with the GR antagonist RU486 (Beck *et al*, 1993; Fig 2A). Similarly, LRH-1 transcriptional activity could be significantly increased by LRH-1 overexpression. As predicted, treatment with 3d2 or SR1848 resulted in a potent inhibition of LRH-1 reporter activity (Fig 2B).

LRH-1 overexpression completely suppressed the basal activity of endogenous GR (Fig 2C, left). Also, the massive dexamethasone-induced reporter activity of overexpressed GR was significantly reduced in response to simultaneous LRH-1 overexpression (Fig 2C, right). Vice versa, dexamethasone-induced activation of the GR resulted in significant LRH-1 inhibition that was comparable to inhibition by 3d2 (Fig 2D).

Based on our findings, we hypothesized that the reciprocal inhibition of GR and LRH-1 results from their interaction-mediated sequestration and should thus correlate with protein expression levels of the respective opponent. Indeed, dexamethasone-induced GR activity significantly declined in a dose-dependent manner in response to co-transfection with increasing amounts of LRH-1 expression plasmid (Fig 2E). Similarly, increasing GR levels caused a dose-dependent reduction of LRH-1 transcriptional activity (Fig 2F). Although spontaneous nuclear translocation of the GR due to overexpression was sufficient to significantly inhibit LHR-1 activity, dexamethasone treatment further enhanced LRH-1 inhibition even at low levels of GR overexpression.

Interestingly, treatment of cells with 3d2 alone already enhanced the activity of endogenous as well as overexpressed GR (Fig 2C),

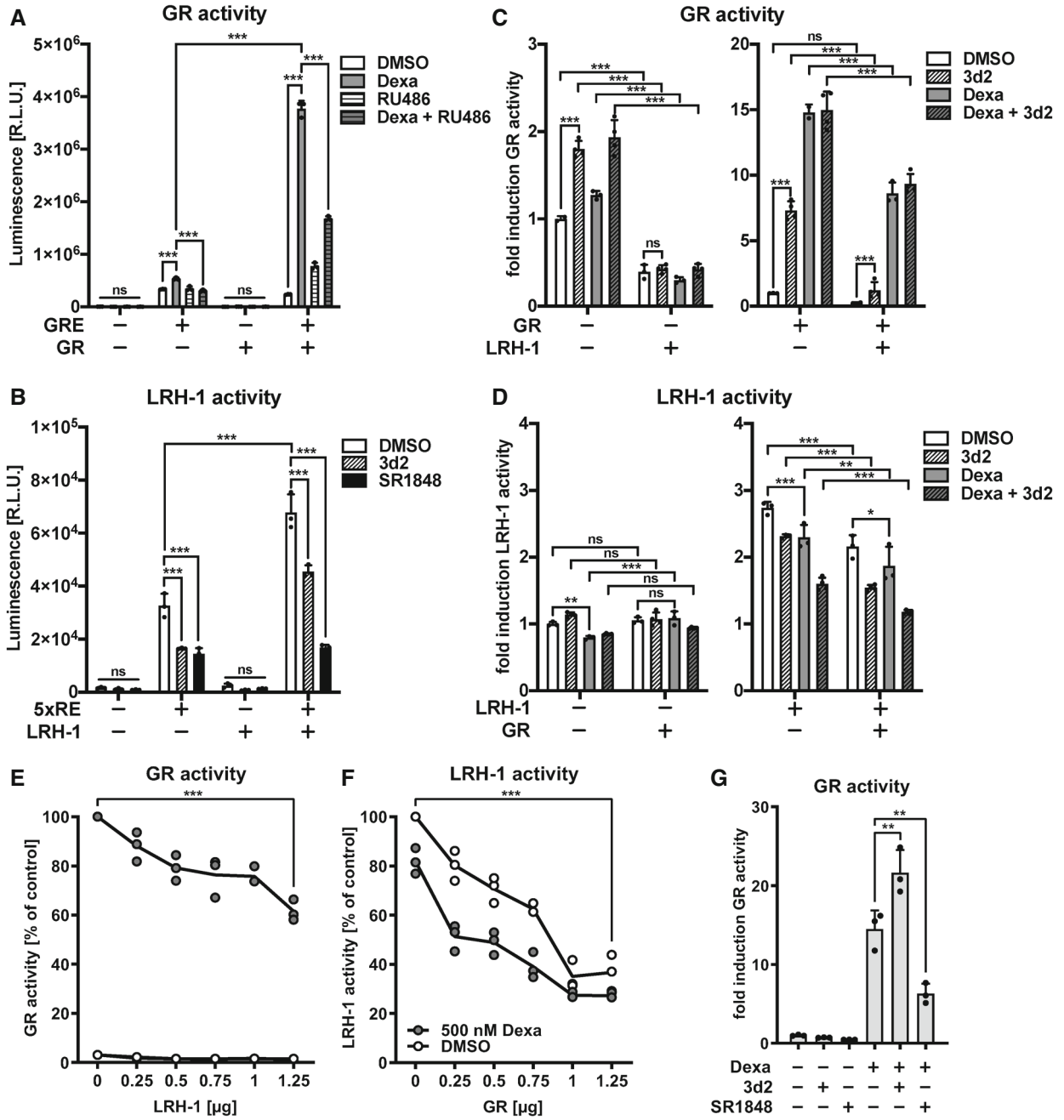

Figure 2. Reciprocal inhibition of the GR and LRH-1.

A–F Quantification of GR and LRH-1 transcriptional activities in HEK 293T cells co-transfected with equal amounts of the GR responsive (GRE) (A, C, E) or LRH-1 responsive (5xRE) (B, D, F) luciferase reporter constructs as well as mh-hGR (GR) and/or mh-hLRH-1 (LRH-1), as indicated. Corresponding empty vectors (represented by: −) were used as negative controls and to adjust the total DNA content in every transfection. β-galactosidase (bGal) was co-transfected as an internal transfection control. Reporter cells were treated overnight with dexamethasone (Dexa), 3d2 and/or SR1848, as indicated. For inhibition of GR activity cells were further pre-treated for 1 h with RU486. Dimethyl sulfoxide (DMSO) was used as solvent control. (A, B) Luciferase reporter activity was measured, and luminescence was normalized to bGal activity (relative light units, R.L.U.). (C, D) Fold induction of transcriptional activities was calculated by further normalization to endogenous GR or LRH-1 activity of DMSO-treated luciferase reporter cells, respectively. (E, F) Numbers indicate percentage (%) of bGal-normalized activities of overexpressed GR (E) and LRH-1 (F) relative to the DMSO-treated controls co-transfected with empty vector instead of LRH-1 or GR, respectively.

G HEK 293T cells transiently transfected with GRE/GR were treated with Dexa, 3d2 and/or SR1848, as indicated by: +. DMSO was used as solvent control (represented by: −). Fold induction of GR activity was calculated by normalization of bGal-normalized luminescence to DMSO-treated reporter cells.

Data information: Mean values of technical triplicates ± SD of a typical experiment ($n \geq 3$ biological replicates) are shown. Two-way ANOVA (A-D), unpaired *t*-test (E/F) or one-way ANOVA (G); ns, not significant, *$P < 0.05$, **$P < 0.01$, ***$P < 0.001$.

suggesting that endogenous LRH-1 restricts basal GR activity. Furthermore, while 3d2 enhanced GR activity, SR1848 caused a reduction of dexamethasone-induced GR activity (Fig 2G). This correlates with the observations that SR1848 strongly reinforces the interaction between GR and LRH-1, whereas 3d2 has rather the opposite effect (Fig 1D).

Cumulatively, these data strongly suggest a mutual antagonism of LRH-1 and the GR that is most likely mediated by their direct, GC-dependent protein–protein interaction. Importantly, it is possible to enhance or repress this physical and regulatory interaction using pharmacological inhibitors, respectively, activators, to modulate the transcriptional activity of both NRs.

GR, LRH-1 and GC resistance in T cell acute lymphoblastic leukemia cells

Closely resembling features of the well-investigated interplay between the GR and NF-κB, respectively, AP-1, we presumed that LRH-1-mediated GR inhibition could possibly impact GC sensitivity. GC resistance is a frequently observed phenomenon in T-ALL cells. We thus chose the three human T-ALL-derived T lymphocyte cell lines, Jurkat, MOLT-4 and CEM-C1, to test this hypothesis. These T-ALL cells are largely unresponsive to the growth-inhibiting and cell death-inducing effects of GCs (Fig 3A and B). Even though affecting proliferation of CEM-C1 cells after prolonged incubation (Fig 3A),

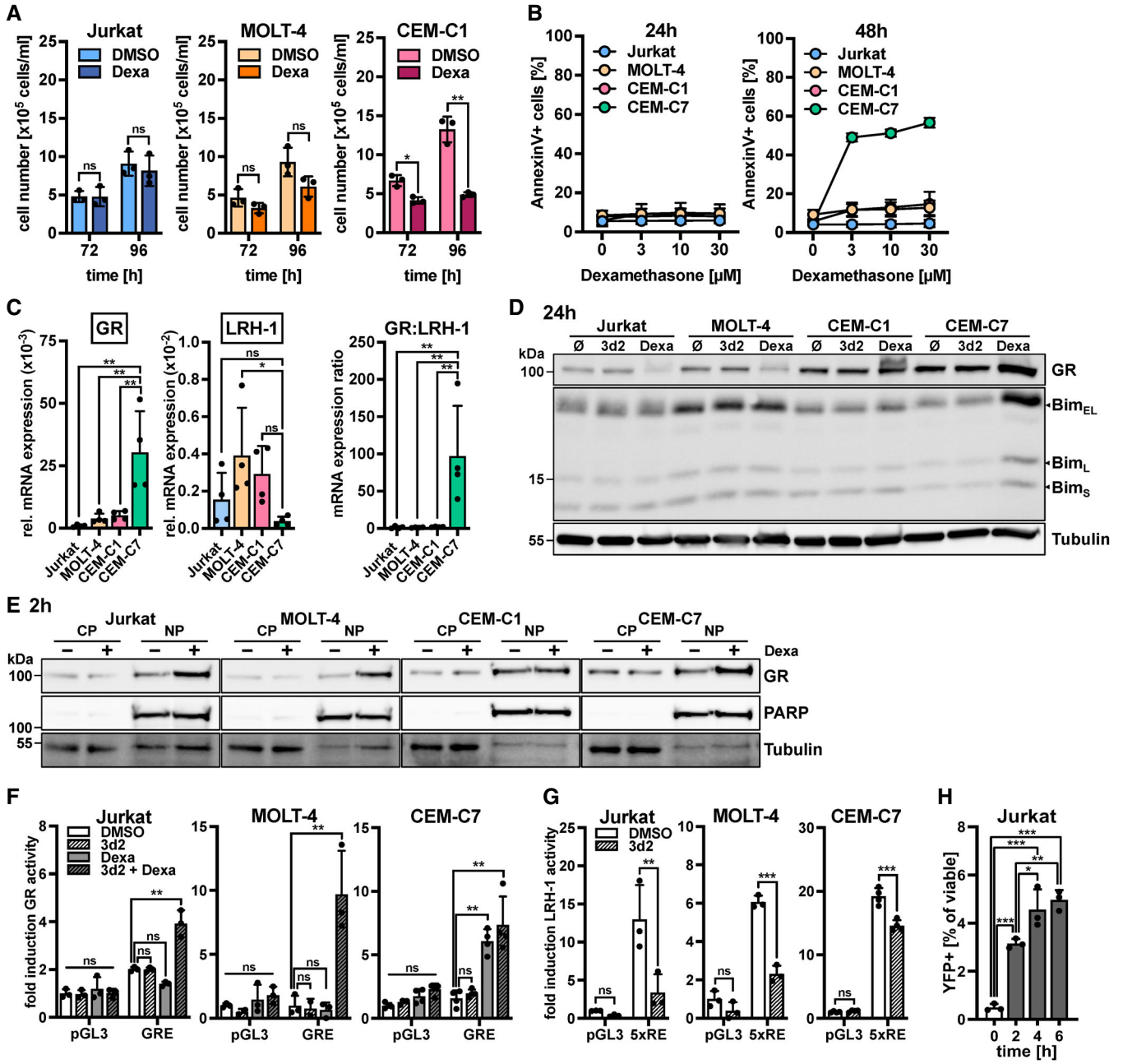

Figure 3.

Figure 3. GR, LRH-1 and GC resistance in T cell acute lymphoblastic leukemia cells.

A Cell count-based comparison of cellular proliferation of T-ALL cells after treatment with dexamethasone (Dexa). Individual and mean values of three biological replicates ± SD analyzed by two-way ANOVA are shown.

B Flow cytometric analysis of cell death by AnnexinV staining in T-ALL cell lines upon treatment with indicated Dexa concentrations. Cell death is represented by the number of AnnexinV positive (AnnexinV+), apoptotic cells as a percentage (%) of total cells. Mean values of $n \geq 4$ biological replicates ± SD are shown.

C Expression levels of human GRα and LRH-1 mRNA in human T-ALL cell lines were determined by probe-based real-time quantitative PCR, calculated as relative expression compared to beta-actin and used to determine the GR:LRH-1 ratio (right). Individual and mean values of four biological replicates ± SD are shown and statistically significant differences between CEM-C7 and GC-resistant cell lines were determined by one-way ANOVA.

D Immunoblots of GR, Bim_{EL}, Bim_L and Bim_S and Tubulin from T-ALL cells treated for 24 h. Representative results from $n = 2$ are shown.

E Immunoblots of GR, PARP (nuclear loading control) and Tubulin (cytoplasmatic loading control) from cytoplasmic (CP) and nucleoplasmic (NP) lysates of T-ALL cells treated with Dexa. Note: Nuclear extracts were more highly concentrated (approx. 6-fold) than cytosolic fractions. Representative results from two are shown.

F, G GR and LRH-1 activity in human T-ALL cells transfected with a control luciferase reporter plasmid (pGL3) and either (F) GR responsive (GRE) or (G) LRH-1 responsive (5xRE) luciferase reporter and treated with 3d2 and/or Dexa. β-galactosidase (bGal) was co-transfected as an internal transfection control. Luciferase reporter activity was normalized to bGal activity and calculated as relative to the DMSO-treated pGL3 control. Individual and mean values analyzed by two-way ANOVA of three biological replicates ± SD are shown for Jurkat and CEM-C7 whereas technical triplicates ± SD of a representative experiment ($n = 3$) are shown for MOLT-4.

H Flow cytometry-based quantification of BiFC in Jurkat cells transiently co-transfected with YFP1-LRH-1 and GR-YFP2 and treated for indicated time periods with Dexa. YFP+ cells are shown as a percentage (%) of viable cells. Individual and mean values ± SD of three biological replicates analyzed by one-way ANOVA are shown.

Data information: For all displayed experiments dimethyl sulfoxide (DMSO; represented by Ø or 0 h) was used as a solvent control. ns, not significant, $*P < 0.05$, $**P < 0.01$, $***P < 0.001$.

high concentrations of dexamethasone (up to 30 μM) did not cause apoptotic cell death in Jurkat, MOLT-4 and CEM-C1 cells as assessed by Annexin V staining (Fig 3B), while the GC-sensitive T-ALL cell line CEM-C7 readily exhibited cell death in response to dexamethasone. Importantly, the expression of the transcriptionally active GRα isoform and LRH-1 was detectable in all GC-resistant T-ALL cell lines (Fig 3C). In contrast to the GC-sensitive CEM-C7 cells (Fig 3B), Jurkat, MOLT-4 and CEM-C1 cells lacked a dexamethasone-induced upregulation of the GR (Fig 3D), even though GR translocation was unimpaired (Fig 3E). GC-resistant T-ALL cells further failed to upregulate the three most prevalent Bim isoforms (Bim_{EL}, Bim_L and Bim_S; O'Connor *et al*, 1998; Sionov *et al*, 2015) upon dexamethasone treatment (Fig 3D), a process known to be critical for GC-induced cell death (Smith & Cidlowski, 2010). In fact, even a GC-mediated reduction of GR protein levels was detected in Jurkat and MOLT-4 cells (Fig 3D).

Of interest, while GC-sensitive CEM-C7 cells showed a high GR:LRH-1 ratio, the opposite was observed in Jurkat, MOLT-4 and CEM-C1 cells (Fig 3C), suggesting that LRH-1-mediated inhibition of the GR might be responsible for GC resistance. However, as neither mRNA nor protein expression necessarily reflects functionality, we also assessed GR and LRH-1 activity in T-ALL cell lines using luciferase reporter assays (Fig 3F and G). In line with the observed sensitivity to GCs (Fig 3B), a strong induction of GR activity could be observed in CEM-C7 cells upon dexamethasone treatment whereas hardly any basal nor GC-induced GR activity could be detected in Jurkat as well as MOLT-4 cells. Notably, simultaneous application of 3d2 caused a striking increase in dexamethasone-induced GR activity in both T-ALL cell lines (Fig 3F). Irrespective of their sensitivity towards GCs, constitutive LRH-1 activity could be detected in human T-ALL cells (Fig 3G). Most importantly, the application of non-toxic 3d2 concentrations resulted in a potent inhibition of LRH-1 in all used cell lines, suggesting that the transcriptional activity of LRH-1 can be pharmacologically targeted in T-ALL cells. Altogether, these data, demonstrating that a combination of dexamethasone and the LRH-1 antagonist 3d2 are able to restore GR activity in otherwise GC-unresponsive human T-ALL cell lines, support the notion that LRH-1 could play a role in GC resistance, and that prevention or disturbance of GR-LRH-1 interaction might sensitize GC-resistant leukemic T cells to dexamethasone-induced cell death. In line with this notion, we have seen that also in Jurkat cells dexamethasone treatment resulted in a time-dependent increase in BiFC, indicating that GR and LRH-1 interact with each other in a glucocorticoid-induced manner also in T-ALL cells (Fig 3H).

LRH-1 is a critical regulator of T-ALL proliferation and survival

Controlling proliferation, pluripotency, stress response pathways and energy metabolism, LRH-1 had been shown to favor tumor progression of a variety of solid cancer types (Nadolny & Dong, 2015). As LRH-1 has vital functions in healthy T lymphocytes (Seitz *et al*, 2019), and its expression as well as transcriptional activity was detected in T-ALL cell lines (Fig 3C and G), we examined whether LRH-1 likewise favors the growth and survival of leukemic T cells.

Already after 24 h of specific pharmacological LRH-1 inhibition using compound 3d2, Jurkat, MOLT-4, CEM-C1 and CEM-C7 cells showed remarkably impaired proliferation when compared to solvent control treated cells (Fig 4A). Similar results were also obtained with the alternative LRH-1 inhibitor SR1848 (Fig EV2A). Strongly emphasizing an essential role of LRH-1 in the regulation of T-ALL viability, we failed to generate LRH-1 knockout cells as the complete removal of LRH-1 protein did not allow for the selection of viable, proliferating cells. Nonetheless, to confirm LRH-1 inhibitor-mediated effects, we employed RNA interference-mediated down-regulation of LRH-1 in T-ALL cells. LRH-1 knockdown by lentiviral-mediated introduction of a short hairpin RNA (shRNA) targeting LRH-1 (shLRH-1) was confirmed by probe-based quantitative PCR (Fig EV2B). Notably, LRH-1 expression was almost completely abolished in CEM-C1, while it was only reduced by 50–60% in Jurkat and MOLT-4 when compared to the non-targeting shRNA control construct (shcontrol). Unfortunately, currently available human LRH-1 antibodies are not sensitive enough to detect the comparably low LRH-1 protein levels in hematopoietic cells by Western blotting, and thus LRH-1 knockdown could not be verified on protein level. Nonetheless, comparable to pharmacological LRH-1 inhibition,

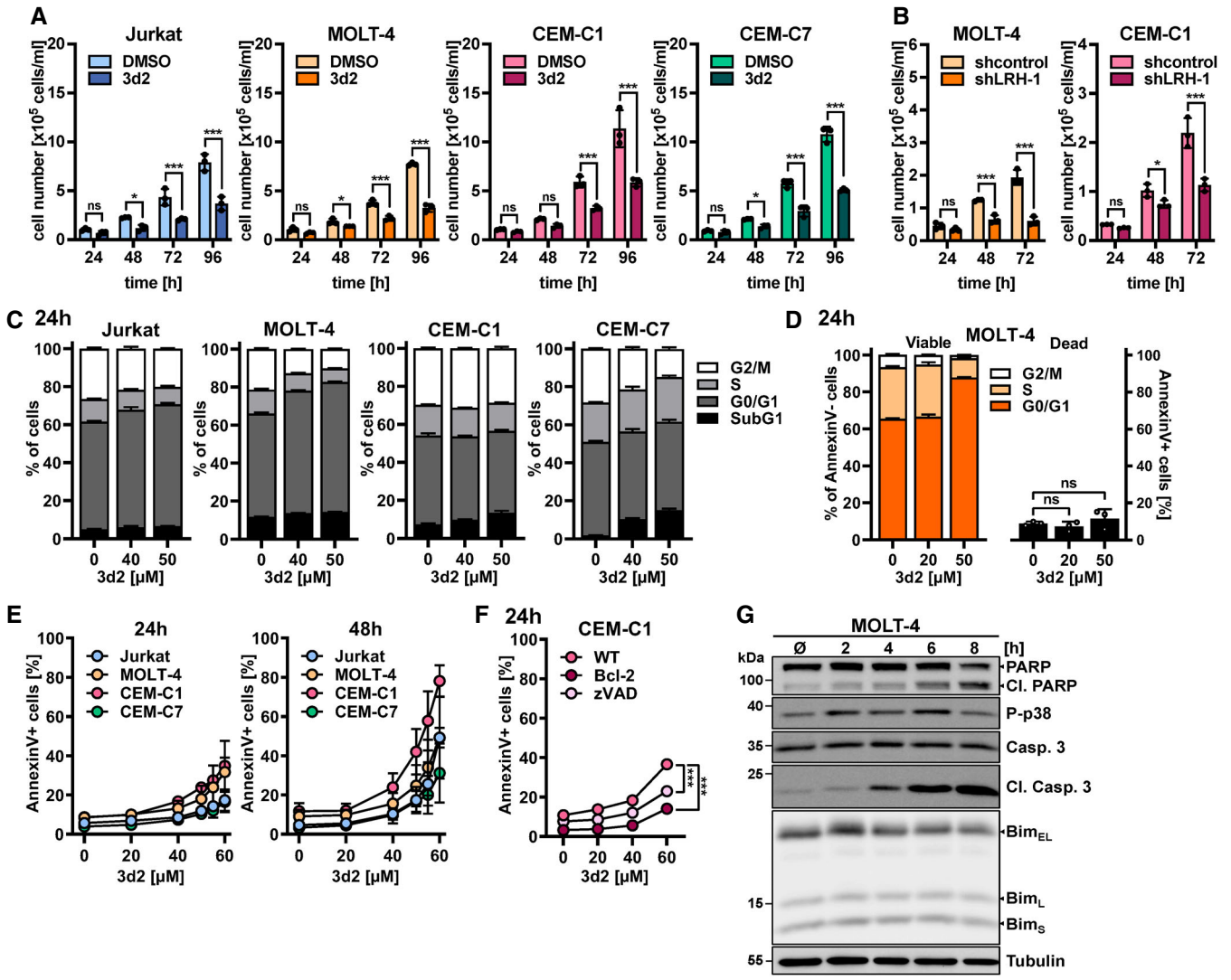

Figure 4. LRH-1 is a critical regulator of T-ALL proliferation and survival.

A, B Daily cell counting-based comparison of cellular proliferation of T-ALL cells after (A) treatment with 3d2 and (B) small hairpin RNA-mediated LRH-1 knockdown (shLRH-1). Individual and mean values of technical triplicates of one representative experiment ($n = 3$) ± SD anlyzed by two-way ANOVA are shown.

C Cell cycle distribution of T-ALL cells treated for 24 h with indicated concentrations of 3d2 as measured by propidium iodide flow cytometry. Representative results from $n = 3$ are shown. Stacked bars represent the mean of technical triplicates ± SD.

D Simultaneous flow cytometric analysis of cell cycle distribution by EdU/DAPI staining and cell death by AnnexinV staining in MOLT-4 cells upon treatment with 3d2. Dead cells are represented by the number of AnnexinV positive (AnnexinV+), apoptotic cells as a percentage (%) of total cells and cell cycle phase distribution as % of viable, AnnexinV negative (AnnexinV−) cells. Representative results from three are shown. Bars represent the mean of technical triplicates ± SD and differences in AnnexinV+ cells were analyzed by one-way ANOVA.

E Flow cytometric analysis of cell death by AnnexinV staining in T-ALL cell lines upon treatment with indicated 3d2 concentrations. Mean values of $n = 4$ ± SD are shown.

F Flow cytometric analysis of 3d2-induced cell death by AnnexinV staining in wild-type (WT), Bcl-2 overexpressing (Bcl-2) and Z-VAD-FMK (zVAD)-treated CEM-C1. Mean values of technical triplicates of one representative experiment ($n = 3$ ± SD analyzed by two-way ANOVA are shown.

G Immunoblots of full-length and cleaved (cl.) PARP, P-p38, c-Myc, Caspase 3 (Casp. 3), cl. Casp. 3, Bim_{EL}, Bim_L and Bim_S and Tubulin from MOLT-4 cells treated with 40 µM 3d2 for indicated time periods. Representative results from two are shown.

Data information: For all displayed experiments dimethyl sulfoxide (DMSO; represented by Ø or 0 h) was used as a solvent control. ns, not significant, $*P < 0.05$, $***P < 0.001$.

LRH-1 knockdown caused a significant growth inhibition in MOLT-4 and CEM-C1 cells (Fig 4B), suggesting that LRH-1 is essential for T-ALL cell proliferation. To gain insight into the underlying molecular mechanism(s), we analyzed the effect of 3d2-mediated LRH-1 inhibition on the expression of c-Myc (Botrugno *et al*, 2004) and cyclin E1 (Xiao *et al*, 2018), two known cell-cycle-regulating LRH-1 target genes. Within 4 h after 3d2 treatment, a strong downregulation of c-Myc and cyclin E1 mRNA expression could be observed in

MOLT-4 as well as CEM-C1 cells (Fig EV2C). Even though short-term LRH-1 inhibition overall caused only minor changes in protein abundance, a slight reduction of both cell cycle regulators could be observed in MOLT-4 after only 2 h and in CEM-C1 cells after 6 h (Fig EV2D). A strong downregulation of c-Myc and cyclin E1 protein levels was further detectable in LRH-1 knockdown T-ALL cells when compared to the corresponding controls (Fig EV2E). In line with this downregulation of cell cycle regulators known to be involved in the G1/S transition (Hume *et al*, 2020), LRH-1 inhibition seemed to impede entry into the cell cycle. 3d2 treatment caused a dose-dependent accumulation of unsynchronized Jurkat and MOLT-4 in the G0/G1 phase (Fig 4C). This was accompanied by a loss of cells in the S and G2/M phase, while the proportion of cells in SubG1, representing apoptotic cells, was not affected after 24 h. In contrast, cell cycle phase distribution of CEM-C1 and CEM-C7 cells remained unaffected by 3d2. This might be explained by their comparably high proliferation rate (Fig 4A) combined with the fact that cells were not synchronized prior to LRH-1 inhibition and mild cytotoxicity of 3d2 at the used concentrations. We could confirm that LRH-1 inhibition blocks the proliferation of T-ALL cells independently of apoptosis induction by combining quantification of dead cells using Annexin V staining with a bidimensional cell cycle analysis of Annexin V-negative, viable cells (Fig 4D). While 24 h treatment with 3d2 did not induce cell death, a strong G1 arrest accompanied by a corresponding reduction of proliferating cells in the S and G2/M phase was observed in MOLT-4 cells. Taken together, these results provide clear evidence for an essential role of LRH-1 in the proliferation or more specifically the G1 to S phase transition of T-ALL cells, likely via the transcriptional control of cell cycle-regulating genes.

Interestingly, when the LRH-1 inhibitor 3d2 was applied at sufficiently high concentrations and for prolonged time, it also induced cell death in T-ALL cells, as measured by Annexin V staining (Fig 4E). Already after 24 h of treatment, 10–35% dead cells could be detected in the different T-ALL cell lines in response to 3d2, which was further enhanced after 48 h of treatment. While prolonged incubation with high 3d2 concentrations triggered cell death in approximately one third of CEM-C7 and half of Jurkat as well as MOLT-4 cells, CEM-C1 cells were exquisitely sensitive to 3d2 and died up to 80%. In contrast, identical concentrations of a 3d2-related control substance (Benod *et al*, 2013), compound 2 (Cpd2), did not show any cell death-inducing effects (Fig EV2F). To further verify the specificity of 3d2-induced cell death, we next tested the cell death-promoting effects of SR1848. Requiring about five- to six-fold lower concentrations (≤10 μM), this small molecule LRH-1 repressor reduced the viability of CEM-C1 and MOLT-4 cells even more potently compared to 3d2 (Fig EV2G). This is in line with previous studies showing that SR1848 inhibits the transcriptional activity of LRH-1 with higher potency (Corzo *et al*, 2015; Schwaderer *et al*, 2017). In contrast, Jurkat cells were completely insensitive towards SR1848 (Fig EV2G), even when applied at much higher concentrations.

Given the fact that not only apoptotic, but also late necrotic cells can be detected by Annexin V staining (Crowley *et al*, 2016), we next wanted to analyze the nature of 3d2-mediated T-ALL cell death. As caspase induction is a hallmark of apoptosis (Saraste & Pulkki, 2000), we first tested whether cell death induction by 3d2 is suppressed upon caspase inhibition. Indeed, treatment with the pan-caspase inhibitor z-VAD-fmk (zVAD) markedly reduced the percentage of 3d2-induced Annexin V-positive CEM-C1 cells (Fig 4F). Furthermore, overexpression of the anti-apoptotic protein Bcl-2 was sufficient to completely rescue CEM-C1 cells from 3d2-induced cell death (Figs 4F and EV2H). Along these lines, a 3d2-induced rapid but transient increase in the pro-apoptotic Bcl-2 family member Bim could be observed after 2 h. This was followed by caspase 3 processing and cleavage of the caspase substrate PARP, which is consistent with the induction of apoptotic cell death (Fig 4G). Even though mild and transient, activation of p38, a stress kinase known to be activated by essentially all environmental stress stimuli (Canovas & Nebreda, 2021), indicates a state of general stress in T-ALL cells early upon 3d2-mediated LRH-1 inhibition.

While early inhibition of LRH-1 with pharmacological inhibitors or when applied at low concentrations mainly impairs proliferation, prolonged treatment with high concentrations of LRH-1 inhibitors (especially 3d2) potently induced T-ALL cell death mediated by activation of intrinsic apoptosis signaling. In summary, the presented results thus highlight the importance of LRH-1 in cell cycle progression as well as the survival of leukemic T cells.

Regulation of GC-induced cell death by LRH-1

With growing evidence that 3d2-mediated LRH-1 inhibition enhances GR activity (Fig 2) by impairing the newly discovered inhibitory GR-LRH-1 interaction (Fig 1), we next aimed to investigate whether interference with LRH-1 may be exploited to sensitize T-ALL cells towards GC-induced apoptosis. Therefore, we first evaluated the effects of the combination of a sublethal concentration of dexamethasone with increasing amounts of 3d2. In all GC-resistant T-ALL cell lines tested, dexamethasone significantly enhanced 3d2-mediated cell death induction (Fig 5A). Interestingly, this effect was most pronounced in MOLT-4 that also exhibited highest LRH-1 mRNA expression (Fig 3C). Furthermore, sublethal concentrations of 3d2 restored dexamethasone sensitivity of MOLT-4 cells in a dose-dependent manner resulting in a strong synergistic cell death induction with up to almost 100% apoptotic cells after 48 h (Fig 5B). Even though significant, only minimal synergistic drug activity could be observed 24 h after combined dexamethasone and 3d2 treatment (Fig EV3A). This correlates with the overall comparably late onset of GC toxicity occurring only after 48 h, as observed in CEM-C7 cells (Fig 3B). To our surprise, 3d2-mediated LRH-1 inhibition not only potently enhanced but also accelerated dexamethasone-induced apoptosis in this GC-sensitive cell line (Fig 5C). Already after 24 h, non-toxic dexamethasone concentrations in combination with 3d2 resulted in a striking, dose-dependent synergy promoting up to 60% cell death. In line with previous experiments, this synergistic effect was even more pronounced after 48 h, when the combined treatment of CEM-C7 cells with 3d2 and dexamethasone concentrations in the low nanomolar range was sufficient to cause maximal cell death induction. This raised the question of whether a prolonged incubation might further enhance the synergistic drug effects in GC-resistant Jurkat, MOLT-4 and CEM-C1 cells. We thus extended the treatment duration from 48 h (Fig 5A) to 72 h, which barely altered the relatively low cell death rates in response to 3d2 or dexamethasone single treatments (Fig 5D). As anticipated, elongation of the treatment, however, notably enhanced the 3d2-mediated sensitization towards dexamethasone of all T-ALL

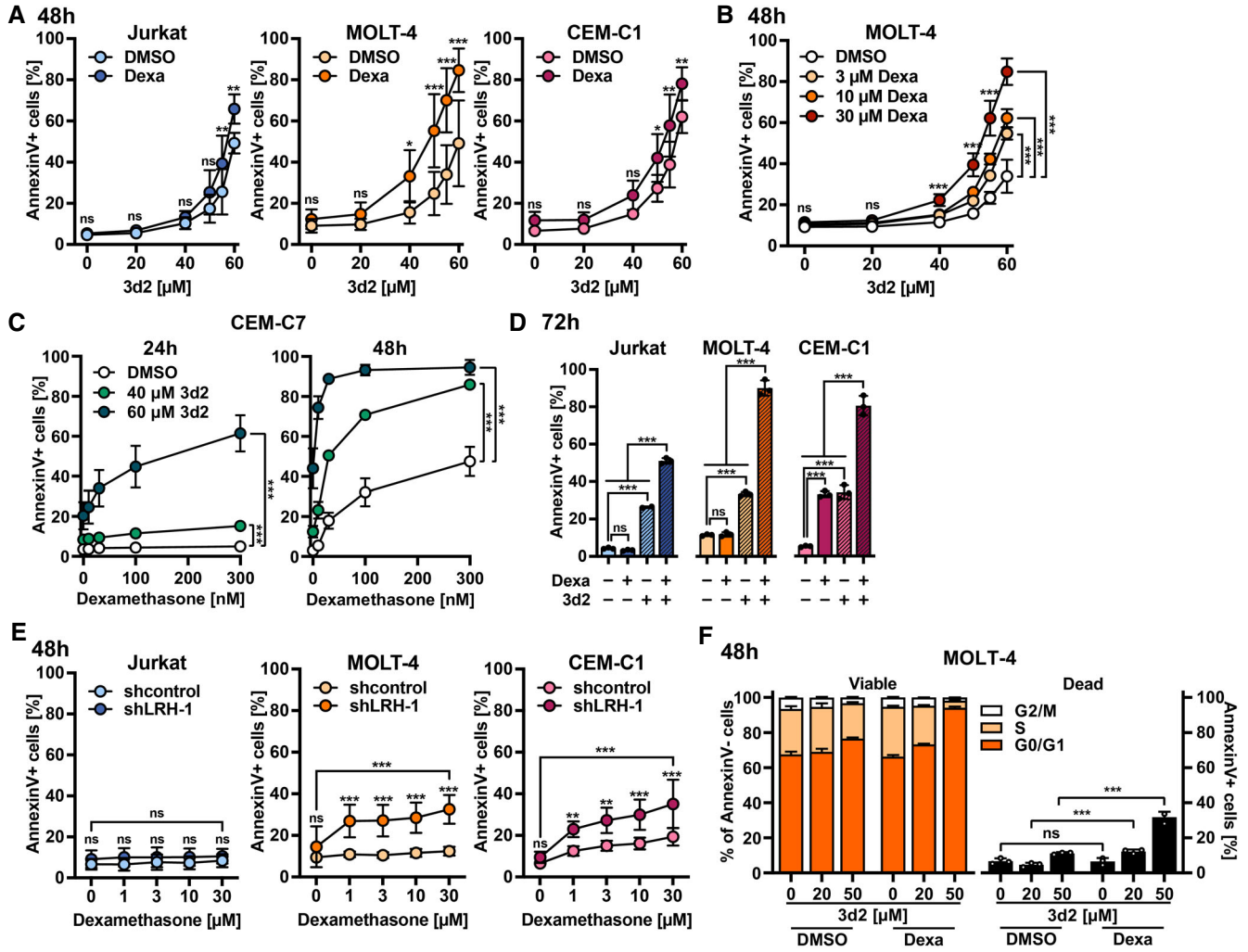

Figure 5. Regulation of GC-induced cell death by LRH-1.

A–D Flow cytometric analysis of cell death by AnnexinV staining in T-ALL cell lines upon treatment with Dexamethasone (Dexa) and 3d2. (A) 30 µM Dexa; (D) 55 µM 3d2 and 30 µM Dexa. Mean values of (A) $n = 4$, (B) technical triplicates of one representative experiment ($n = 4$), (C) $n = 3$ and (D) technical triplicates of one representative experiment ($n = 3$) ± SD are shown.

E Flow cytometric analysis of cell death by AnnexinV staining in T-ALL cell lines expressing a non- (shcontrol) or LRH-1 (shLRH-1) targeting small hairpin RNA construct and treatment with 30 µM Dexa. Mean values of $n = 3$ ± SD are shown.

F Flow cytometric analysis of cell cycle distribution by EdU/DAPI staining and cell death by AnnexinV staining in MOLT-4 cells upon treatment with 30 µM Dexa and 3d2. Dead cells are represented by the number of AnnexinV positive (AnnexinV+), apoptotic cells as a percentage (%) of total cells and cell cycle phase distribution as % of viable, AnnexinV negative (AnnexinV−) cells. Representative results from $n = 3$ are shown. Bars represent the mean of technical triplicates ± SD.

Data information: For all displayed experiments dimethyl sulfoxide (DMSO; represented by − or 0) was used as a solvent control. Two-way ANOVA (A–C, E) and one-way ANOVA (D, F); ns, not significant, *$P < 0.05$, **$P < 0.01$, ***$P < 0.001$.

cell lines tested and thus resulted in massive synergistic cell death induction.

Confirming the specificity of 3d2-mediated sensitization towards GC induced apoptosis, we could show that the control substance Cpd2 did not synergize with dexamethasone in any T-ALL cell line tested (Fig EV3B and C). Even more importantly, LRH-1 knockdown (shLRH-1) significantly sensitized MOLT-4 and CEM-C1 cells towards dexamethasone-induced cell death when compared to the corresponding control (Fig 5E). Similar as in experiments using 3d2, the dose-dependent increase in Annexin V-positive LRH-1 knockdown cells was especially pronounced 48 h after dexamethasone application even though significant, but mild effects were already observed after 24 h (Fig EV3D). In contrast, shLRH-1-expressing Jurkat cells remained completely resistant towards GC-induced apoptosis (Fig 5E) despite a reduction of LRH-1 mRNA expression in comparison to the corresponding control could be verified by RT-qPCR (Fig EV2B).

Given the opposing roles of LRH-1 and the GR in cell cycle regulation of (leukemic) T cells, we next addressed whether a combination of 3d2 and dexamethasone also synergistically impairs T-ALL proliferation. Indeed, almost all cells that survived synergistic apoptosis induction (viable, AnnexinV-negative) accumulated in the G1

phase in response to the combination of dexamethasone and 3d2, as exemplarily shown in MOLT-4 cells (Fig 5F). Accordingly, barely any viable cells were detected in the S and G2/M phase, suggesting that 3d2-mediated LRH-1 inhibition and GCs cooperatively prevent G1/S transition in T-ALL cells. In line with the results described above (Figs 3A and 4D), a notable but comparably mild G1 arrest could also be observed after 3d2 single treatment while dexamethasone alone did not affect MOLT-4 cell proliferation.

Taken together, these results indicate that LRH-1 contributes to GC resistance and further show that its synthetic antagonist 3d2 not only possesses anti-leukemic potential as a single agent, but also cooperates with GCs to harm leukemic T cells by synergistically inducing apoptosis and cell cycle arrest.

Sensitization to GC-induced cell death by 3d2 is mediated by improved upregulation of Bim

Despite extensive research, the exact molecular mechanisms underlying GC sensitivity and thus also resistance remain incompletely resolved. It is, however, well-established that GC-induced cell death in healthy and malignant lymphocytes critically relies on activation of the intrinsic mitochondrial apoptosis pathway involving GR-mediated upregulation of the pro-apoptotic Bcl-2 family member Bim (Jing *et al*, 2015). Accordingly, GC resistance in T-ALL could be linked to an impaired ability to induce Bim expression (Bachmann *et al*, 2007). In line with this, Bim protein levels remained unchanged when MOLT-4 cells were treated with dexamethasone while a modest Bim protein induction could be observed after 3d2-mediated LRH-1 inhibition (Fig 6A). However, combining dexamethasone with increasing 3d2 concentrations triggered a marked, dose-dependent increase of Bim protein levels and consequently also PARP cleavage, suggesting induction of mitochondrial apoptosis signaling. In line with this, caspase inhibition using zVAD-FMK rescued MOLT-4 cells not only from 3d2 single toxicity but also from the synergistic cytotoxicity of 3d2 in combination with dexamethasone (Fig 6B).

To gain further information on the role of Bim in 3d2-mediated sensitization to GC-induced apoptosis, we generated Bim knockout T-ALL cell lines using CRISPR/Cas9 (Fig EV4A and B). Compared to the corresponding control, Bim-deficient CEM-C7 cells were completely rescued from apoptosis induced by the combination of dexamethasone and 3d2(Fig 6C). Also after prolonged treatment (48 h) Bim deficiency significantly protected CEM-C7 cells against this synergistic drug activity and prevented cell death induction by high 3d2 concentrations applied as a single agent. (Fig EV4C). Similar results were obtained in MOLT-4 cells (Fig EV4D). In comparison to CEM-C7 cells, these effects were, however, far less pronounced as residual Bim protein expression was detected in Bim knockout MOLT-4 cells (Fig EV4B). Nonetheless, these results suggest the essential contribution of Bim in 3d2-induced apoptosis and especially in the 3d2-mediated sensitization to GCs in T-ALL cells. Given that higher levels of Bim were detected in LRH-1 knockdown cells (Fig 6D), it is possible that LRH-1 negatively regulates Bim expression and/or abundance in a direct or indirect manner. Concurrently, reduced LRH-1 expression was accompanied by a decrease in Bcl-2 protein levels. Thus, altered ratios of Bim and Bcl-2 may contribute to increased GC sensitivity, as recently shown in leukemia cells (Jing *et al*, 2015).

It is well-established that lymphotoxic GC effects not only rely on GR-mediated gene induction, such as auto-upregulation of the GR and induction of Bim, but also on non-genomic, GR-independent signaling pathways (Clarisse *et al*, 2020). We thus deleted the GR from T-ALL cells to determine whether its presence is required or dispensable for the synergistic cell death induction by GCs and 3d2 (Fig EV4E and F). A profound protection from apoptosis was observed in GR-deleted MOLT4 cells treated with dexamethasone plus 3d2 (Figs 6E and EV4G), indicating that GR signaling is required for the synergistic induction of cell death in T-ALL cells. Interestingly, even cell death induced by 3d2 alone was reduced in GR-deficient cells, suggesting that LRH-1 inhibition may facilitate endogenous GR signaling in MOLT4 cells. In line with previous studies showing that the GR critically regulates Bim expression in a direct (Jing *et al*, 2015) or indirect manner (Heidari *et al*, 2012), GR deficiency was accompanied by decreased Bim RNA levels (Fig EV4F). Vice versa, knockdown of LRH-1 increased the basal GR mRNA expression threefold and further improved the upregulation of the GR in response to dexamethasone when compared to the corresponding control cell line (Fig 6F). Similarly, LRH-1 knockdown CEM-C1 cells expressed higher Bim mRNA under basal conditions, and prolonged treatment with dexamethasone induced a drastic increase in Bim mRNA expression compared to control cells (Fig 6G). After 24 h, this improved transcriptional upregulation also clearly translated into increased protein levels of Bim in MOLT-4 (Fig 6H) and CEM-C1 cells (Fig EV4H). Silencing of LRH-1 resulted also in increased basal and GC-induced GR protein levels in CEM-C1 cells (Fig EV4H), while this effect was less pronounced in MOLT-4 cells (Fig 6H). Whereas at this early time point (24 h) increased dexamethasone-induced GR and Bim expression could be observed, only little caspase activation as monitored by caspase 3 and PARP cleavage could be detected (Figs 6H and EV4H), but synergistic induction of cell death by dexamethasone in LRH-1-silenced cells became evident after 48 h (Fig 5E).

In line with a role of LRH-1 in the regulation of energy metabolism via the transcriptional regulation of glutaminase 2 (GLS2) and glucokinase (GCK; Oosterveer *et al*, 2012; Xu *et al*, 2016), increased phosphorylation of the AMP-activated protein kinase (AMPK) was observed in LRH-1-silenced or 3d2-treated cells (Figs 6H and EV4H) suggesting increased metabolic stress due to lower cellular ATP levels. Increased activation of AMPK was paralleled by reduced c-Myc levels (Figs 6H and EV4H), likely resulting in the reduced proliferation detected in 3d2-treated or LRH-1-silenced cells. Similar to other cancer types (Michalek & Brunner, 2020), LRH-1 is thus also a critical regulator of metabolic pathways and associated energy production in T-ALL cells.

In summary, these data support the idea that synergistic cell death induction by dexamethasone and 3d2 treatment is executed by the intrinsic, mitochondrial apoptosis pathway involving Bcl-2 family members and caspase activation. Importantly, pharmacological LRH-1 inhibition and LRH-1 downregulation yielded comparable results, supporting the specificity of 3d2. Both, pharmacological inhibition and LRH-silencing promoted T-ALL sensitization to GCs by restoring GR activity (Fig 3E) and associated induction of the pro-apoptotic BCL-2 member Bim. Moreover, activation of AMPK suggests a role of LRH-1 in the energy production of leukemic T cells.

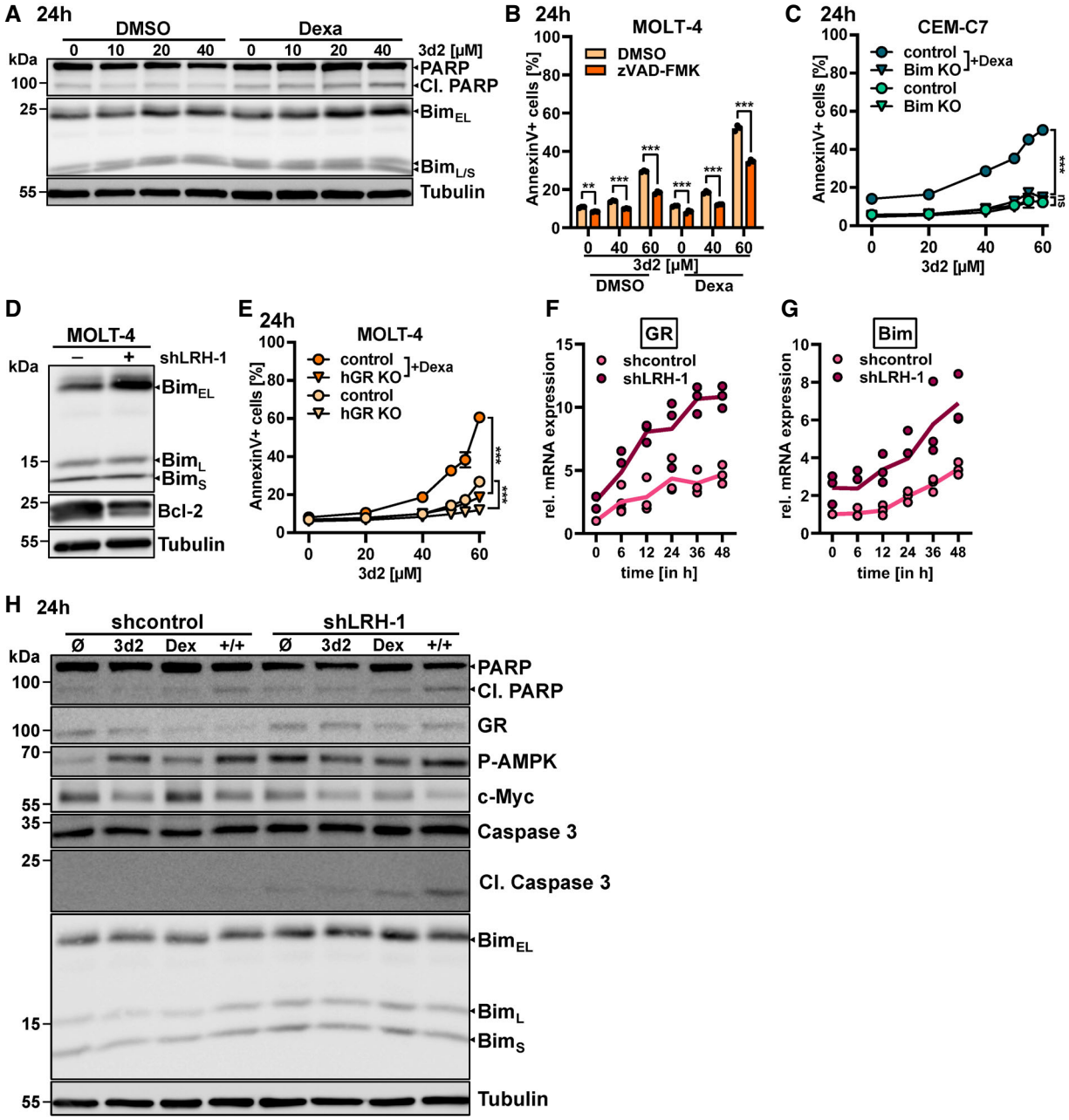

Figure 6. Sensitization to GC-induced cell death by 3d2 is mediated by improved upregulation of Bim.

A Immunoblots of full-length and cleaved (cl.) PARP, Bim_{EL}, Bim_L and Bim_S and Tubulin from MOLT-4 cells treated for 24 h with 10 µM dexamethasone (Dexa) and 3d2. Representative results from three are shown.

B Flow cytometric analysis of cell death by AnnexinV staining in MOLT-4 cells treated with 3d2, 30 µM Dexa and/or 50 µM pan caspase inhibitor Z-VAD-FMK (zVAD). Individual and mean values of technical triplicates of one representative out of $n = 3 \pm$ SD are shown.

C Flow cytometric analysis of cell death by AnnexinV staining in control or Bim knockout (Bim KO) CEM-C7 cells treated with 3d2 and 30 µM Dexa. Mean values of technical triplicates of one representative of $n = 4 \pm$ SD are shown.

D Immunoblots of Bim_{EL}, Bim_L and Bim_S, Bcl-2 and Tubulin from MOLT-4 expressing a non- (shcontrol) or LRH-1- (shLRH-1) targeting small hairpin RNA construct.

E Flow cytometric analysis of cell death by AnnexinV staining in control or glucocorticoid receptor knockout (GR KO) MOLT-4 cells treated with 3d2 and 30 µM Dexa. Mean values of $n = 3 \pm$ SD are shown.

F, G mRNA expression levels of human GR (F) and Bim (G) in shcontrol and shLRH-1 CEM-C1 cells were determined by real-time quantitative PCR after treatment with 1 µM Dexa for indicated times. Fold induction relative to the untreated shcontrol sample (0 h) was calculated after normalization to beta-actin. Individual values of technical triplicates of one representative of two ± SD are shown.

H Immunoblots of full-length and cleaved (cl.) PARP, GR and phospho-AMPK (P-AMPK), c-Myc, full-length and cl. Caspase 3, Bim_{EL}, Bim_L and Bim_S and Tubulin from MOLT-4 cells treated with 40 µM 3d2 and/or 10 µM Dexa. Representative results from two are shown.

Data information: For all displayed experiments dimethyl sulfoxide (DMSO; represented by 0 or Ø) was used as a solvent control. Two-way ANOVA (B, C, E); ns, not significant, $^{**}P < 0.01$, $^{***}P < 0.001$.

Synergistic cell death induction by 3d2 and dexamethasone in patient-derived human T-ALL

Thus far, our data strongly suggest that LRH-1 is not only essential for the proliferation and survival of T-ALL cells but seems also to be critically involved in the regulation of GC sensitivity due to a protein–protein interaction-mediated inhibition of the GR. To address the relevance of these findings in T-ALL patient samples, we next assessed the effect of 3d2-mediated LRH-1 inhibition on dexamethasone sensitivity in human T-ALL patient-derived xenografts (PDX), which closely recapitulate the genetic landscape of primary leukemic T cells (Frismantas *et al*, 2017; Richter-Pechańska *et al*, 2018). Primary human T-ALL PDX, co-cultured *ex vivo* on mesenchymal stromal cells, were treated for 72 h with increasing concentrations of 3d2 and dexamethasone in a matrix-based assay. Cell viability was subsequently analyzed using an imaging-based fluorescence readout as described previously (Frismantas *et al*, 2017; Fig 7A). 3d2 applied as a single agent did not affect the viability of the majority of the T-ALL samples. Nevertheless, in one out of the four tested T-ALL PDX (Sample 2) more than 2 μM 3d2 was sufficient to notably reduce cellular viability. Similarly, patient-derived cells were insensitive to GCs alone, except for sample 2, in which dexamethasone single treatment reduced the cellular viability by almost 60%. Most importantly, however, combined treatment of human PDX cells with 3d2 and dexamethasone resulted in synergistic induction of cell death in most samples tested. Excitingly, approximately 1,000 times lower concentrations of dexamethasone than in T-ALL cell lines were sufficient to promote synergistic cell death induction (Fig 7A), suggesting that primary T-ALL cells respond particularly well to the combination of 3d2 and dexamethasone. Accordingly, an additive or even synergistic activity of dexamethasone and 3d2 could be confirmed in 75% of the in total 8 primary T-ALL samples tested as indicated by synergy score (Z-score) values above 0 (Fig 7B). In some T-ALL samples (e.g. Samples 2 and 3) a striking synergy between dexamethasone and 3d2 was observed, as already low nanomolar 3d2 concentrations resulted in maximal cell death. In contrast, dose-dependent, intermediate synergistic effects or a complete lack of cell death induction was observed in other PDXs, as exemplified by Sample 1 and Sample 4, respectively (Fig 7A). Analysis of mRNA transcript levels revealed differential GR, LRH-1 and Bim expression in individual T-ALL patient samples (Fig 7C). Noteworthy, a remarkably high GR:LRH-1 expression ratio was observed in leukemia cells that were not only resistant to the combined treatment but which, on the contrary, even caused antagonistic effects as indicated by Z-scores below 0 in Samples 4 and 8 (gray bars). In line with this observation, drug responsiveness represented by Z-scores negatively correlated with GR:LRH-1 expression ratios (Fig 7D). Positive correlations between Z-scores and LRH-1 as well as Bim expression levels, on the other hand, provide further evidence for the LRH-1 specificity of 3d2, and Bim being a critical mediator of cell death-induced by the combined treatment with dexamthasone.

Given the promising anti-leukemic effects of the combination of 3d2 and dexamethasone in cell lines as well as *ex vivo* cultured PDX, we wanted to further assess the potential clinical application of these findings. Even though we demonstrated that 3d2 does not exhibit single dose toxicity *in vivo* while having potent beneficial effects in acute T cell as well as macrophage-mediated hepatitis models (Schwaderer *et al*, 2017, 2020), up to date there are no published data regarding the long-term efficacy, adverse effects or cumulative toxicity of 3d2 in mammals. To test the therapeutic potential of long-term 3d2 treatment alone or in combination with GCs *in vivo*, we conducted a small-scale pre-clinical *in vivo* experiment employing two of the *ex vivo* tested primary T-ALL samples in a xenograft model. To further reduce the sample size, we did single mouse testing. This approach almost equals conventional methods for predicting drug responses but only employs one immunodeficient mouse injected with PDX cells per treatment condition (Murphy *et al*, 2016). In short, after a three-week treatment with dexamethasone and/or 3d2 injections every two or five days, respectively, leukemia engraftment was monitored over time by determining the proportion of human CD45+ hematopoietic cells in the peripheral blood using flow cytometry. The two patient-derived tumor samples showed quite different growth behavior *in vivo* (Fig 7E). While Sample 2 resulted in an already very high tumor burden after 40 days, Sample 1 required more than 60 days for notable tumor engraftment. First and foremost, no obvious general toxicity nor adverse drug reactions as documented by increased weight loss were observed after long-term and repeated *in vivo* administration of 3d2, suggesting a relatively good safety profile. Somewhat unexpectedly, the response to combined dexamethasone and 3d2 treatment *in vivo* did only partially correlate with the intermediate and strong *in vitro* synergy for Sample 1 and Sample 2, respectively (Fig 7A). Despite lacking sensitivity *ex vivo*, single agent dexamethasone and 3d2 treatment delayed the *in vivo* leukemia progression of both T-ALL patient-derived tumor cells to some extent, but eventually resulted in a similar tumor burden as in control treated animals. Most importantly, the combination of dexamethasone and 3d2 synergistically reduced the accumulation of human leukemia cells in the peripheral blood after transplantation of PDX Sample 1. In comparison to the single agents alone, combined LRH-1 inhibition and GR activation not only drastically prolonged survival by more than 20 days but also seemed to ultimately result in leukemia regression. Contrary to expectations based on the strong synergistic effects *in vitro*, combination therapy only transiently delayed *in vivo* leukemia progression of the highly aggressive primary T-ALL cells from patient Sample 2.

In conclusion, these PDX-based *ex vivo* and *in vivo* experiments confirm our *in vitro* data suggesting an essential role of LRH-1 in proliferation, survival and GC responsiveness of human T-ALL cells in the majority of samples tested. Thus, LRH-1 inhibitor-based sensitization of tumor cells to GC-induced cell death may represent an interesting novel therapeutic approach for the treatment of T-ALL, at least in a subset of patients.

Discussion

Transcription factors of the NR superfamily have diverse regulatory functions in a wide variety of biological processes via the transcriptional control of complex gene regulatory networks (Kininis & Kraus, 2008). Since a deregulation of their activity is linked to various diseases, NRs represent interesting therapeutic targets, and current research thus aims at the design and characterization of compounds that specifically stimulate or repress NR activity. Apart from ligand-binding, heterodimerization with other transcription

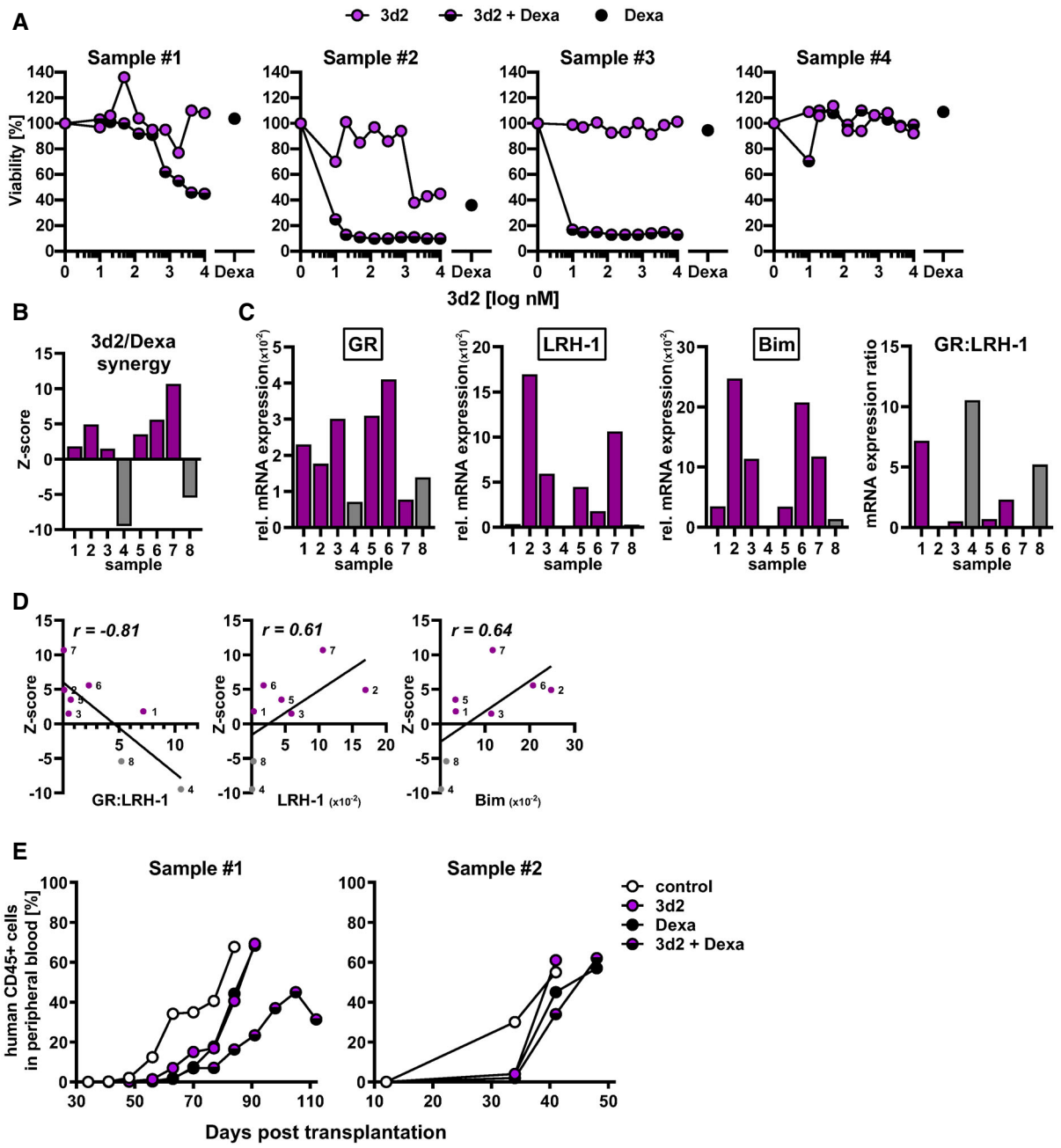

Figure 7. Synergistic cell death induction by 3d2 and dexamethasone in patient-derived human T-ALL.

A *Ex vivo* response of human T cell acute lymphoblastic leukemia (T-ALL) patient-derived xenografts (PDX), co-cultured on hTERT-immortalized primary bone marrow MSCs, to treatment with indicated concentrations of 3d2 and/or dexamethasone (Sample 1, 3 and 4: 1 nM; Sample 2: 0.1 nM). Cell viability was quantified by fluorescent live cell staining using CyQuant combined with automated image analysis (Frismantas *et al*, 2017) and calculated as percentage (%) of the dimethyl sulfoxide treated control.

B Synergy scores (Z-scores) between 3d2 and dexamethasone of human T-ALL patient-derived xenografts (PDX) were calculated from the viability curves of PDX samples treated with increasing concentrations of 3d2 and/or dexamethasone using SynergyFinder tool. Z-scores ≥0 indicate additivity or synergism and < 0 antagonism.

C Expression levels of human GRα, LRH-1 and Bim mRNA in human human PDX were determined by real-time quantitative PCR, calculated as relative expression compared to beta-actin and used to determine the GR:LRH-1 ratio (right).

D Pearson correlation coefficients (*r*) calculated between Z-scores shown in (B) and the GR:LRH-1 expression ratio as well as Bim mRNA levels from (C).

E *In vivo* leukemia progression of human T-ALL PDX transplanted into NSG mice treated for 3 weeks with vehicle (PBS control), 40 mg/kg 3d2 and or 10 mg/kg Dexamethasone starting 3 days post transplantation. Engraftment was calculated as % of human vs total (human+mouse) CD45 positive (CD45+) cells as assessed by flow cytometric analysis of peripheral blood.

Data information: All displayed experiments display one biological replicate.

factors, including other NRs, has been shown to critically contribute to the regulation of NR activity, further increasing the range and complexity of individual NR target gene networks and regulation (Amoutzias *et al*, 2007; Weikum *et al*, 2018). Particularly well-described in this context are the direct physical interactions of the GR with NF-κB, respectively, AP-1, that are primarily responsible for the immune-suppressive effects of GCs by transrepressing these two pro-inflammatory transcription factors (Schule *et al*, 1990; Liden *et al*, 1997; Liberman *et al*, 2018). However, the direct protein–protein interactions with these survival-promoting transcription factors result also in GR sequestration, and thus restriction of the GC-initiated cell death-inducing activity of the GR, which mainly relies on its transcriptional activity (de Bosscher *et al*, 2003). Here we report a novel heterodimeric interaction of the GR with LRH-1 with important consequences for their respective transcriptional activities. Importantly, this physical and regulatory interaction was found to be specifically modulated by small molecule LRH-1 inhibitors to selectively increase or repress GR activity. While 3d2-mediated LRH-1 inhibition reduces antagonistic GR-LRH-1 interactions, consequently resulting in increased GR activity, SR1848 significantly reinforces interactions between LRH-1 and GR, and associated transrepression due to the translocation of LRH-1 to the cytoplasm.

LRH-1 and GR have fundamentally opposing regulatory functions in immune cells. Therefore, the reciprocal antagonism of the GR, and LRH-1 is most likely implicated in various physiological and pathophysiological processes involving immune cells and interactions with tissue cells. Only recently, LRH-1 expression, function and pharmacological targetability could be unequivocally confirmed in hematopoietic cells (Benod *et al*, 2013; Schwaderer *et al*, 2017; Schwaderer *et al*, 2020; Seitz *et al*, 2019). Even though lymphocytes exhibit rather low LRH-1 expression levels in comparison to other tissues (Bookout *et al*, 2006; Seitz *et al*, 2019; Uhlén *et al*, 2015), LRH-1 is indispensable for T cell development and function (Seitz *et al*, 2019). The critical role of LRH-1 in T cells is emphasized by the observation that LRH-1 deletion in tissues with high LRH-1 expression, such as the liver and the intestine, does not cause any tissue-specific developmental defects (Mataki *et al*, 2007; Lee *et al*, 2008), whereas T cell-specific LRH-1 deletion results in a drastic reduction of mature peripheral T lymphocytes, and strongly impaired activation-induced proliferation and effector functions of the remaining T cells (Seitz *et al*, 2019). Consequently, LRH-1-deficient T cells fail to promote intestinal inflammation in a transfer model of experimental colitis (Seitz *et al*, 2019), illustrating the importance of LRH-1 in regulating T cell proliferation and pro-inflammatory effector functions. In line with this notion, LRH-1 is also expressed at low levels in T-ALL cells (Fig 3C), yet is critically involved in the regulation of proliferation and survival of GC-resistant T-ALL cells (Figs 3 and 4). Thereby confirming the proposed oncogenic properties of LRH-1 (Michalek & Brunner, 2020), we suggest that LRH-1 represents an interesting therapeutic target in the treatment of T cell leukemias.

In contrast to LRH-1, GR activation suppresses T cell proliferation and T cell-mediated inflammation, in part also by promoting T cell apoptosis. Activation-induced LRH-1 expression therefore likely also limits the anti-proliferative and cell death-promoting activity of the GR. Due to their strong immunomodulatory and cell death-promoting actions, synthetic GCs are among the most prescribed drugs, and current mainstay in the therapy of inflammatory and auto-immune diseases, as well as hematopoietic malignancies, including T-ALL (Hodgens & Sharman, 2022; Pearson & Eliel, 1950). As the therapeutic potential of GCs is, however, severely limited by the high incidence of primary or secondary GC resistance with ill-defined underlying molecular mechanisms, there is an urgent need for new therapeutic options and targets to effectively treat T-ALL (Olivas-Aguirre *et al*, 2021). By pharmacological inhibition and RNA interference experiments, we obtained comprehensive data that LRH-1 inhibition targets GC-resistant T-ALL cells at various levels. (i) By reducing the expression of c-Myc and cyclin E1, two well-known LRH-1 target genes that regulate G1/S transition (Botrugno *et al*, 2004; Xiao *et al*, 2018; Hume *et al*, 2020), LRH-1 inhibitors strongly impair the proliferation of leukemic T cells (Figs 4 and EV2). (ii) Furthermore, at higher concentrations, LRH-1 inhibition by 3d2 activates the intrinsic apoptosis pathway involving upregulation of Bim, caspase 3 activation and PARP cleavage (Fig 4E–G). (iii) Most importantly, we show that antagonism of LRH-1 restores GC sensitivity, resulting in synergistic induction of cell death upon treatment of T-ALL cells by 3d2 and dexamethasone (Fig 5). Highlighting the potential clinical relevance of LRH-1-mediated suppression of GR signaling and GC resistance also in primary human patient samples, we could demonstrate that the majority of PDX cells responded by increased cell death induction upon combined treatment with 3d2 and dexamethasone (Fig 7).

Our data suggest several molecular mechanisms underlying this synergistic induction of cell death, with the most relevant one presumably being the 3d2-mediated disruption of the antagonistic GR-LRH-1 complex (Fig 1D). Consequently, by restoring GR activity in the GC resistant T-ALL cell lines (Fig 3F) 3d2 facilitates initiation of the mitochondrial apoptosis signaling pathway in response to GCs, thereby enhancing dexamethasone sensitivity of GC-resistant and sensitive T-ALL cell lines (Fig 5). Since GR auto-induction and Bim upregulation were shown to be critical for GC-mediated cell death (Ramdas *et al*, 1999), which was observed in GC-sensitive but not resistance T-ALL cell lines (Fig 3D), many combination therapy approaches aim at re-establishing these processes. For example, reversal of GC resistance by the mTOR (mammalian target of rapamycin) inhibitor Rapamycin (Lopez-Royuela *et al*, 2010; Guo *et al*, 2013) or the protein synthesis inhibitor Anisomycin critically relies on the cooperative upregulation of GR and Bim (Liu *et al*, 2014). Our results indicate that the synergistic drug activity of dexamethasone and 3d2 is analogously based on improved GR activaton as well as upregulation and Bim induction (Figs 3F and 6). Together with the observation that GR deletion protects from 3d2-mediated re-sensitization towards dexamethasone (Figs 6E and EV4G) our data demonstrate that the presence of transcriptionally active GR is a fundamental prerequisite for GC-induced cell death (Brown & Ferrando, 2018). Interestingly, GR deletion also rescued from 3d2 single toxicity. This suggests that apoptosis induction by 3d2 may involve activation of endogenous GR signaling due to the release of the GR from LRH-1-mediated sequestration (Figs 6E and EV4G). In this respect, it has been interesting to observe that dexamethasone-induced apoptosis is enhanced in LRH-1-deficient thymocytes (S. Michalek, T. Brunner, unpublished observation). Thus, antagonistic LHR-1-GR interactions seem to play comparable roles in the regulation of proliferation and cell death induction in primary and malignant T cells.

Despite the general heterogenicity of patient-derived leukemia cells (Clarisse *et al*, 2020), we observed an additive or in many cases even synergistic reduction in cell viability in most *ex vivo* cultured human PDX samples after combined treatment using low doses of dexamethasone and 3d2 (Fig 7A and B). Even more remarkable, a synergistic delay of leukemia progression could also be observed in a corresponding *in vivo* PDX T-ALL engraftment model (Fig 7E). This up-to-date unique long-term and repeated application of LRH-1 inhibitors, in general, and 3d2, in particular, provides further very first evidence for the relative safety of systemic treatment with LRH-1 inhibitors. Despite the limited sample size, these experiments with human PDX tumor cells emphasize the clinical significance of the newly discovered GR-LRH-1 interaction in the context of pathophysiological GC resistance and confirm an important role of LRH-1 in the regulation of leukemic T cell viability. Furthermore, correlation analysis revealed that GR:LRH-1 expression ratios, as well as LRH-1 and Bim expression are a good predictors for the synergistic induction of cell death by 3d2 and dexamethasone (Fig 7D). However, future studies must further complement our so far limited, but promising initial results, and validate how critical LRH-1-mediated GR sequestration is in general in mediating GC resistance in T-ALL patients.

Taken together, we discovered a novel GC-dependent direct physical interaction of the GR with LRH-1 that results in transrepression of both nuclear receptors and that mediates GC resistance. Specific LRH-1 inhibitors can be used to modulate the GR-LRH-1 interaction and mutual antagonism to selectively restore or repress GR activity and associated GC sensitivity. Furthermore, LRH-1 was found to be a critical regulator of T-ALL cell proliferation and survival. Thus, our findings may also have important implications for the design and development of innovative LRH-1 inhibitor-based therapeutic approaches to delay leukemia progression and re-sensitize T-ALL cells towards GCs and possibly also other chemotherapeutic drugs.

Materials and Methods

Reagents and Tools Table

Reagent/Resource	Reference or source	Identifier or catalog number
Experimental models		
E. coli DH5α for plasmid preparation	Previous hosting lab	N/A
E. coli Stbl3 for cloning of lentiCRISPRv2 constructs	Previous hosting lab	N/A
E. coli XL-1 blue supercompetent for cloning of split-YFP constructs	Previous hosting lab	N/A
Patient-derived xenografts *(H. sapiens)*	B. Bornhauser	N/A
CEM-C1 *(H. sapiens)*	ATCC	Cat# CRL-2265; RRID:CVCL_3496
CEM-C1 Bcl-2 *(H. sapiens)*	Brumatti *et al* (2008)	N/A
CEM-C1 shcontrol *(H. sapiens)*	This study	N/A
CEM-C1 shLRH-1 *(H. sapiens)*	This study	N/A
CEM-C7 control KO *(H. sapiens)*	This study	N/A
CEM-C7 hGR KO *(H. sapiens)*	This study	N/A
CEM-C7-14 (CEM-C7) *(H. sapiens)*	Bornhauser *et al* (2007)	RRID:CVCL_6825
HEK 293H *(H. sapiens)*	Thermo Fisher Scientific	Cat# 11631017; RRID:CVCL_6643
HEK 293T *(H. sapiens)*	ATCC	Cat# CRL-3216; RRID:CVCL_0063
hTERT-immortalized mesenchymal stroma cells (MSC) *(H. sapiens)*	Mihara *et al* (2003)	N/A
Jurkat *(H. sapiens)*	ATCC	Cat# TIB-152; RRID:CVCL_0367
Jurkat shcontrol *(H. sapiens)*	This study	N/A
Jurkat shLRH-1 *(H. sapiens)*	This study	N/A
MOLT-4 *(H. sapiens)*	ATCC	Cat# CRL-1582, RRID:CVCL_0013
MOLT-4 Bim KO *(H. sapiens)*	This study	N/A
MOLT-4 control KO *(H. sapiens)*	This study	N/A
MOLT-4 GR KO *(H. sapiens)*	This study	N/A
MOLT-4 shcontrol *(H. sapiens)*	This study	N/A
MOLT-4 shLRH-1 *(H. sapiens)*	This study	N/A
NSG mouse strain (NOD.*Cg-Prkdc*^{scid} *Il2rg*^{tm1Wjl}/SzJ) *(M. musculus)*	The Jackson Laboratory	Cat#005557
Recombinant DNA		
pcDNA3.1 Myc/His (+) A (pcDNA)	Invitrogen	V80020
GRE_2-tk-luc (GRE)	Liden *et al* (1997)	N/A

Reagents and Tools table (continued)

Reagent/Resource	Reference or source	Identifier or catalog number
lentiCRISPRv2	Addgene (Sanjana *et al*, 2014)	Cat# 52961
lentiCRISPRv2 gEGFP	This study	N/A
lentiCRISPRv2 human Bim	This study	N/A
lentiCRISPRv2 human GR	This study	N/A
pRSV-Rev	Gift from Marco Herold	Addgene Cat# 12253
pMDLg/pRRE	Gift from Marco Herold	Addgene Cat# 12251
pMD2.G	Gift from Marco Herold	Addgene Cat# 12259
TKpGL3 LRH-1-RE 5x (5xRE)	Schoonjans *et al* (2002)	N/A
pGL3 basic (pGL3)	Promega	Cat# E1751
MISSION® pLKO.1-puro Non-Mammalian shRNA Control Plasmid DNA (shcontrol)	Sigma-Aldrich	Cat# SHC002
NR5A2 MISSION® shRNA Plasmid DNA (shLRH-1)	Sigma-Aldrich	Cat# SHCLND-NM_003822
pcDNA3.1_YFP1_L_hLRH-1 (YFP1-LRH-1)	This study	N/A
pDsRed2-N1-GR (dsRed GR)	This laboratory	(Backbone: Takara Bio Cat# 632406)
pEGFP-LRH-1	This laboratory	N/A
pcDNA3.1_hGR (GR)	This laboratory	N/A
pcDNA3.1_hLRH-1 (LRH-1)	This laboratory	N/A
pcDNA3.1_bGal (bGal)	This laboratory	N/A
pcDNA3.1_GR_L_YFP2 (GR-YFP2)	This study	N/A
pcDNA3.1_YFP1_L_hGR (YFP1-GR)	This study	N/A
pcDNA3.1-CCR7-YFP2	Gift from D. Legler (Hauser *et al*, 2016)	N/A
pcDNA3.1-YFP1-N-term	Gift from D. Legler	N/A
pEGFP-C1	Clontech	N/A (discontinued)
Antibodies		
Rabbit mAB anti-Bcl2	Cell Signaling Technology	Cat# 2870; RRID:AB_2290370
Rabbit mAB anti-Bim	Cell Signaling Technology	Cat# 2933, RRID:AB_1030947
Rabbit pAB anti-Caspase3	Millipore	Cat# 235412; RRID:AB_2259557
Rabbit pAB anti-Cleaved Caspase 3	Cell Signaling Technology	Cat# 9661; RRID:AB_2341188
Rabbit mAB anti-CyclinE1	Cell Signaling Technology	Cat# 20808; RRID:AB_2783554
Mouse mAB anti-GFP	Roche	Cat# 11814460
Rabbit mAB anti-GR	Cell Signaling Technology	Cat# 12041; RRID:AB_2631286
Rabbit mAB anti-MYC	Cell Signaling Technology	Cat# 13987; RRID:AB_2631168
Rabbit mAB anti-PARP	Cell Signaling Technology	Cat# 9532; RRID:AB_659884
Rabbit mAB anti-phospho-AMPK (Thr172)	Cell Signaling Technology	Cat# 2535; RRID:AB_331250
Rabbit mAB anti-phospho-p38	Cell Signaling Technology	Cat# 4631; RRID:AB_331765
Mouse mAB anti-Tubulin	Sigma-Aldrich	Cat# T5168; RRID:AB_477579
Mouse mAB APC anti-humanCD45 (anti-hCD45)	BioLegend	Cat# 304011; RRID:AB_314399
Rat mAB Brilliant Violet 510(TM) anti-mouseCD45 (anti-mCD45)	BioLegend	Cat# 103137; RRID:AB_2561392
Mouse FITC anti-humanCD7 (anti-hCD7)	BioLegend	Cat# 982704; RRID:AB_2650638
Oligonucleotides and other sequence-based reagents		
Primer sequences cloning of split YFP-constructs	This study (Metabion)	Table EV1
Primer sequences RT-qPCR	This study (Metabion)	Table EV2
sgRNA sequences	This study (Metabion)	Table EV3
Chemicals, enzymes and other reagents		
Adenosine 5-triphosphate (ATP)	Roth	Cat# K029.2

Reagents and Tools table (continued)

Reagent/Resource	Reference or source	Identifier or catalog number
Co-Enzyme A	PJK	Cat# 102211
cOmplete™, EDTA-free Protease Inhibitor Cocktail (protease inhibitor)	Roche	Cat# 04693132001
Compound 2 (Cpd2)	ChemBridge Corp	ID: 7826747
Compound 3d2 (3d2)	ChemBridge Corp	ID: 16728690
D-Luciferine Na salt (Luciferin)	PJK	Cat# 102132
DAPI	BioLegend	Cat# 422801
Dexamethasone	Sigma-Aldrich	Cat# D4902
DNase I (RNase-free)	New England BioLabs	Cat# M0303
FastAP Thermosensitive Alkaline Phosphatase	Thermo Fisher Scientific	Cat# EF0654
FastDigest Buffer (10x)	Thermo Fisher Scientific	Cat# B64
FastDigest Esp3I (BsmBI)	Thermo Fisher Scientific	Cat# FD0454
Fluorescein isothiocyanate (FITC)-labeled AnnexinV	This study	N/A
Fluoroshield™ with DAPI	Sigma-Aldrich	Cat# F6057
Hoechst 33342	Invitrogen™	Cat# H1399
Lumino	Fluka	Cat# 09253
Ni Sepharose 6 Fast Flow L	GE Healthcare	Cat# 17–5,318-01
O-nitrophenyl-β-D-galactopyranoside (ONPG)	Roth	Cat# CN.22
p-Coumaric acid	Sigma-Aldrich	Cat# C-9008
Polybrene (Hexadimethrine bromide)	Sigma-Aldrich	Cat# H9268
Polyethylimine (PEI)	Polysciences	Cat# P3143
Propidium Iodide (PI)	Sigma-Aldrich	Cat# P4864
Puromycin.2HCl	Enzo Life Sciences	Cat# BML-GR312
Restriction enzyme: ClaI	New England BioLabs	Cat# R0197
Restriction enzyme: EcoRI	New England BioLabs	Cat# R3101
Restriction enzyme: XbaI	New England BioLabs	Cat# R0145
Restriction enzyme: XhoI	New England BioLabs	Cat# R0146
RNA-Solv®	Omega Bio-Tek	Cat# R6830
RU486 (Mifepriston)	TOCRIS	Cat# 1479
SR1848	Sigma-Aldrich	Cat# SML 1513
T4 DNA Ligase	New England BioLabs	Cat# M0202
T4 DNA Ligase Reaction Buffer	New England BioLabs	Cat# B0202S
T4 PNK	New England BioLabs	Cat# M0201S
TriFast™	VWR	Cat# 30–2030
zVAD-FMK	Selleck Chemials Llc	Cat# S7023
Software		
Advanced cell Classifier	Misselwitz *et al* (2010)	N/A
AxioVision Software	Carl Zeiss Microscopy	SE64 Rel.4.8
BD FACSDiva	BD Biosciences	V6.2
Cell Profiler™	Broad Institute	http://cellprofiler.org/
CRISPR design tool *(no longer available)*	Zhang Lab, Cambridge, MA	crispr.mit.edu
FlowJo	FlowJo LLC	V10.7
ImageJ	Wayne Rasband, NIH, US	1.48v
Prism	GraphPad Software	V6.0
StepOnePlus™ Software	Thermo Fisher	v2.3
SyngeryFinder web application (V2.0)	Ianevski *et al* (2017)	https://synergyfinder.fimm.fi/synergy/20210603104758451136/

Reagents and Tools table (continued)

Reagent/Resource	Reference or source	Identifier or catalog number
ZEN Software	Carl Zeiss Microscopy	N/A
Other		
Gene Pulser/MicroPulser Electroporation Cuvettes, 0.2 cm gap	Bio-Rad Laboratories	Cat# 1652086
LentiCRISPRv2 target guide sequence cloning protocol	Addgene	https://media.addgene.org/cms/filer_public/4f/ab/4fabc269-56e2-4ba5-92bd-09dc89c1e862/zhang_lenticrisprv2_and_lentiguide_oligo_cloning_protocol_1.pdf
647 EdU Click Proliferation Kit	BD Biosciences	Cat# 565456; RRID: AB_2869678
Amaxa® Cell Line Nucleofector® Kit L (MOLT-4)	Lonza	Cat# VCA-1005
Amaxa® Cell Line Nucleofector® Kit V (Jurkat)	Lonza	Cat# VCA-1003
CyQUANT Cell Proliferation	Thermo Fisher	Cat# C7026
Fast SYBR Green master mix	Applied Biosystems	Cat# 4334973
High capacity cDNA Reverse Transcription Kit	Applied Biosystems	Cat# 4368814
NucleoSpin Plasmid (no lid), Mini kit for plasmid DNA	Macherey-Nagel	Cat# 740499
Phusion® High-Fidelity PCR Kit	New England BioLabs	Cat# M0553
Pure Yield™ Plasmid Midiprep System	Promega	Cat# A2495
QIAquick Gel Extraction Kit	Qiagen	Cat# 28706X4
QIAquick PCR Purification Kit	Qiagen	Cat# 28104
Quick Ligation™ Kit	New England BioLabs	Cat# M2200
Venor®GeM Classic	Minerva Biolabs	Cat# 11–1050
VolcanoCell 2G RT-PCR 2x Master Mix	myPOLS Biotec	N/A
AXIO Observer.Z1 Microscope	Zeiss	N/A
BD LSRFortessa™ cell analyzer (incl. High throughput sampler)	BD Biosciences	N/A
Image Quant LAS 4000	GE Healthcare	N/A
Infinite® 200 PRO series	TECAN	N/A
Nanodrop 2000 spectrophotometer	Thermo Scientific	N/A
peQStar 2X Gradient PCR (thermocycler)	peQLab	N/A
StepOnePlus real- time PCR System	Thermo Fisher	N/A

Methods and Protocols

Patient-derived xenografts

Patient-derived xenografts (PDX) used in this study were generated as described (Schmitz *et al*, 2011) by intrafemoral injection of 1×10^5 to 5×10^6 viable primary ALL cells in NSG (NOD.*Cg-Prkdc*^{scid} *Il2rg*^{tm1Wjl}/SzJ; Charles River, Wilmington, USA) mice. Primary cells were obtained from patients recruited in ALL-BFM 2000. Written informed consent had been obtained from all the patients and the experiments conformed to the principles set out in the WMA Declaration of Helsinki and were carried out under approval 2014–383 issued by the cantonal ethics commission of the Kanton Zurich, Switzerland.

Transplanted mice included both male and female animals at the age of 5–8 weeks. Animals were housed in individually ventilated cages with access to food and water *ad libitum*. Leukemia progression was monitored in the peripheral blood by flow cytometry using anti-mCD45, anti-hCD45 and anti-hCD7 (BioLegend, San Diego, USA) antibodies. PDX cells were harvested from the spleen when engraftment reached 75% in the peripheral blood and subsequently cryopreserved in 90% FCS (Invitrogen, Waltham, USA)/10% DMSO (Sigma-Aldrich, St. Louis, USA). *In vivo* experiments were approved by the veterinary office of the Canton of Zurich (license number 131/19), in compliance with ethical regulations for animal research.

Cell lines

The human T cell acute lymphoblastic leukemia cell lines (T-ALL) Jurkat (male), MOLT-4 (male) and CEM-C1 (female) and human embryonic kidney HEK 293 T cells (female) were taken from a previous hosting lab and originally purchased from American Type Culture Collection (ATCC). The parental human T-ALL cell line CEM-C7-14 (referred to as CEM-C7; female) was described previously by (Bornhauser *et al*, 2007) and HEK 293H cells (female) were kindly provided from Jörg Hartig (Konstanz; purchased from Thermo Fisher Scientific, Waltham, USA). CEM-C1 cells over-expressing Bcl-2 as described by (Brumatti *et al*, 2008) were kindly provided by Henning Walczak (Cologne, Germany). Cell lines were tested for mycoplasma contamination using the Venor®GeM Classic kit according to the manufacturers' protocol (Minerva Biolabs, Berlin, Germany). Via 3rd generation lentivirus-mediated introduction of shRNA or CRISPR/Cas9 constructs and following selection with 1 µg/ml puromycin, stable control (shcontrol) and LRH-1 (shLRH-

1) knockdown as well as eGFP (control), GR and Bim knockout (KO) T-ALL cell lines were generated from parental Jurkat, CEM-C1, CEM-C7 and MOLT-4 cells as described in the following METHOD AND PROTOCOLS section. Parental as well as genetically modified T-ALL cells were cultured in Roswell Park Memorial Institute (RPMI) 1640 and HEK 293T/H in Dulbecco's Modified Eagle's Medium (DMEM). All cell culture media were supplemented with 5% fetal bovine serum (FCS), 2 mM L-glutamine and 50 μg/ml gentamicin (all from Sigma-Aldrich). Cells were grown at 37°C and 5% CO_2 in a humidified atmosphere and passaged every 2–3 days. HEK 293T and HEK 293H cells were passaged at 80–90% confluency and T-ALL cell line cultures were started at a density of 1×10^5 viable cells/ml for normal passaging and 3×10^5 viable cells/ml 1 day prior to experiments or lentiviral transduction. hTERT-immortalized mesenchymal stroma cells (MSC) were cultured in RPMI (Invitrogen) containing 10% FCS (Invitrogen).

Plasmids

The GR luciferase reporter plasmids GRE_2-tk-luc (abbreviated GRE) and LRH-1 luciferase reporter (5xRE) have been described previously (Liden *et al*, 1997; Schoonjans *et al*, 2002). The empty control vector pGL3 basic was purchased from Promega (Mannheim, Germany). The Myc/6xHis-tagged GR, LRH-1 and bGal expression plasmids were generated by cloning human GR, LRH-1 and bGal into a pcDNA3.1 Myc/His (+) A expression vector (Invitrogen). dsRed-tagged GR and eGFP-tagged LRH-1 were generated by cloning human GR and LRH-1 in the pDsRed2-N1 (Takara Bio; Mountain View, USA) and pEGFP-C1 (Clontech, France; now Takara Bio), respectively.

Split YFP-tagged constructs for BiFC were obtained by cloning human GR and LRH-1 sequences into BiFC vectors, kindly provided by D. Legler (BITg, Kreuzlingen, Switzerland). Split YFP plasmids (pcDNA3_YFP1-N-Term & pcDNA3_C-term-YFP2) have been previously described (Nyfeler *et al*, 2005; Hauser *et al*, 2016) and are basically pcDNA3.1 vectors (Invitrogen) containing the YFP fragment 1 (YFP1; amino acids 1–157) or fragment 2 (YFP2; amino acids 158–239) fused to a flexible 10-amino acid $(GGGGS)_2$ linker in their 5′ (pcDNA3_C-term-YFP2) or 3′ (pcDNA3_YFP1-N-Term) position. According to the manufacturer's protocols (New England BioLabs, Ipswich, USA), pcDNA3_YFP1-N-Term was digested with *NotI/XbaI* and pcDNA3_C-term-YFP2 with *EcoRI/ClaI*, before plasmids were dephosphorylated using FastAP Thermosensitive Alkaline Phosphatase (Thermo Fisher Scientific), run on an agarose gel and subsequently purified using the QIAquick Gel Extraction Kit (Qiagen, Hilden, Germany). Similarly, full-length human GR and LRH-1 were PCR-amplified using the Phusion® High-Fidelity PCR Kit (New England Biolabs) and primer pairs depicted in Table EV1. PCR products were purified using QIAquick PCR Purification Kit (Qiagen), enzymatically digested and gel purified. Digested backbones and inserts were ligated at a 1:3 ratio using T4 DNA Ligase plus buffer (New England BioLabs) and via heat shock transformed into XL-1 blue supercompetent *E. coli* that were plated to ampicillin-containing LB agar plates. Single colonies were picked, grown in LB medium and plasmids purified using NucleoSpin Plasmid Mini kit for plasmid DNA (Machery-Nagel, Düren, Germany) were sent for sequencing (Eurofins Genomics, Konstanz, Germany).

A 3rd generation lentiviral packaging and envelope system consisting of the pMDLg/pRRE, pRSV-Rev and pMD2.G was used for production of lentiviruses (kindly provided by Marco Herold, Melbourne; Addgene, Watertown, USA). For CRISPR/Cas9-mediated gene deletion, single guide RNA (sgRNA) sequences (listed in Table EV3) were designed using the MIT CRISPR design tool (www.crispr.mit.edu, discontinued). In short, sgRNA oligos targeting eGFP (control), human GR and Bim were duplexed and phosphorylated using T4 PNK (New England Biolabs), ligated into the *BsmBI*-digested lentiCRISPRv2 backbone (Addgene) and transformed into Stbl3 *E. coli* according to the Zhang lab protocol (Sanjana *et al*, 2014). Commercially available plasmids for small hairpin RNA-mediated LRH-1 and control knockdown, NR5A2 MISSION® shRNA Plasmid DNA (shLRH-1) and MISSION® pLKO.1-puro Non-Mammalian shRNA Control Plasmid DNA (shcontrol), were purchased from Sigma-Aldrich.

All plasmids were amplified in *E. coli* DH5α, subsequently purified using the Promega Pure Yield™ Plasmid Midiprep System, analyzed using a NanoDrop 2000 spectrophotometer (Thermo Fisher Scientific) and stored at −20°C.

Transfection

For bimolecular fluorescence complementation and lentivirus production, HEK 293T and HEK 293H cells were transiently transfected using PEI according to the jetPEI® *in vitro* DNA Transfection Protocol (Polyplus-transfection® SA, Illkirch, France). For luciferase reporter assays, co-localization and co-precipitation experiments classic calcium phosphate transfection (Kingston *et al*, 2003) was used. One day prior to transfection, 2.2×10^6 or 3×10^5 HEK 293T cells were seeded in 10 cm dishes (10 ml medium) or 6-well plates (2 ml medium/well). After 24 h, cells were transfected with 2–20 μg total plasmid, depending on the plate format. To minimize basal translocation of the GR due to serum steroids or the pH indicator phenol red (Picard & Yamamoto, 1987) during BiFC, luciferase reporter, co-localization and –precipitation assays, transiently transfected HEK 293T/H cells were cultured in dedicated assay medium. This was prepared by supplementing phenol red-free DMEM with 5% charcoal-stripped (steroid-free) FCS, 2 mM L-glutamine and 50 μg/ml gentamicin.

For luciferase reporter assays, T-ALL cells were transiently transfected via electroporation. Therefore, Jurkat, MOLT-4 and CEM-C7 cells were first gently washed with PBS (100 *g*/10 min). Immediately afterwards, a total of 1.0×10^6 cells per transfection were combined with 4 μg plasmid in total (2 μg YFP1-LRH-1 and 2 μg GR-YFP-2, 3.6 μg luciferase reporter plasmid and 0.4 μg of bGal plasmid) in 100 μl Nucleofector™ Solution V or L (Lonza, Basel, Switzerland), respectively, and transferred to a Gene Pulser/MicroPulser Electroporation Cuvette (Bio-Rad, Hercules, USA). According to the manufacturers' optimized protocol, cells were electroporated using program X-005 and C-005 on an Amaxa Nucleofector™ 2b Device (Lonza). Electroporated cells were transferred into a full RPMI medium and directly distributed to 96-well cell culture plates at a density of 1×10^6 cells/ml and 2×10^5 cells/well.

Generation of stable LRH-1 knockdown, GR and Bim knockout T-ALL cell lines

For the production of lentiviruses, 2.2×10^6 HEK 293T cells were transfected with 5 μg pMDLg/pRRE, 2.5 μg pRSV-Rev and 3 μg pMD2.G as well as 10 μg lentiCRISPRv2 gEGFP, lentiCRISPRv2 human Bim, lentiCRISPRv2 human GR, MISSION® pLKO.1-puro

Non-Mammalian shRNA Control Plasmid DNA or NR5A2 MISSION® shRNA Plasmid DNA. After 24 h, lentiviral particles were harvested by filtration of the virus-containing medium using a 0.45 μm filter. One milliliter was added to 2 ml T-ALL cells seeded at 3×10^5 cells/ml in a 6-well plate. Fresh full DMEM was added to virus-producing HEK 293T cells and after additional 24 h of virus production, viral supernatants were similarly harvested and another 1–2 ml added to the corresponding target cells. To enhance the transduction efficiency polybrene (Sigma-Aldrich) was added at a final concentration of 4 μg/ml. Starting the next day, successfully transduced T-ALL cells were selected by culture in full RPMI supplemented with 1 μg/ml puromycin (Enzo Life Sciences, Lörrach, Germany). After 1 week, the puromycin selection pressure was removed and stable control (shcontrol) and LRH-1 (shLRH-1) knockdown as well as eGFP (control), GR (GR KO) and Bim (Bim KO) knockout T-ALL cell lines were expanded for 3–4 days in standard RPMI, before being subjected to further experiments. LRH-1 knockdown, GR and Bim knockout efficiencies were verified by quantitative real-time PCR (qPCR) and/or immunoblot analysis as described below.

Pharmacological compounds and treatment of cell lines

The LRH-1 antagonist compound 3d2 (ID: 16728690) and corresponding control compound 2 (ID: 7826747) were synthesized according to the initial publication from Benod *et al* (2013) by ChemBridge Corp (San Diego, USA). SR1848 (SML 1513) and dexamethasone (D4902) were purchased from Sigma-Aldrich, and RU486 from Tocris Bioscience (BioTechne, Wiesbaden-Nordenstadt, Germany; 1479). zVAD-FMK was purchased from Selleck Chemicals Llc (Houston, USA; S7023). Stock solutions of chemical compounds were kept as 20 mM Stock solution in DMSO and stored at −20 or −80°C. Figure legends specify duration of treatments as well as concentrations of compounds used for individual experiments.

In vivo treatment

Recipient animals ($n = 4$ per PDX sample) were transplanted with 1×10^6 PDX ALL cells by tail vein injection. 3 days after transplantation, animals were randomized and treated with either vehicle (PBS, daily), 40 mg/kg 3d2 in PBS (2× a week), 10 mg/kg Dexamethasone in PBS (daily) or the combination of 40 mg/kg 3d2 (2× per week) and 10 mg/kg Dexamethasone (daily) for 3 weeks. Leukemia progression was monitored by flow cytometry of peripheral blood obtained upon tail vein bleeding using anti-hCD45, anti-hCD7 and anti-mCD45 (all purchased from BioLegend). Engraftment was calculated by percentage human vs. human plus mouse CD45 positive cells.

Ex vivo treatment of co-cultured patient-derived xenografts

Primary PDX cells were cultured on hTERT-immortalized primary bone marrow MSCs in 384-well plates as described previously (Frismantas *et al*, 2017). MSCs at 2.5×10^3 per well were plated in 30 μl AIM-V medium 24 h before adding 2×10^4 PDX ALL cells in 27.5 μl of medium. Compounds were reconstituted in DMSO (10 mM stock concentrations) and stored at −80°C. Serially diluted drug concentrations (3d2: 1–10 μM; dexamethasone: 1–10 μM for Sample 1/3 and 0.0001–1 μM for Sample 2/4; DMSO: solvent control) were prepared using a digital dispenser (D300e Digital Dispenser; Tecan). After 72 h incubation, cells were viably stained using a CyQUANT Cell Proliferation kit (Thermo Fisher) and imaged on an ImageXpress Micro (Molecular Devices, San Jose, US) equipped with a CoolLSNap HQ camera (Photometrics, Tucson, US) and a 10x Plan Fluor objective with 0.3 NA (Nikon). Images were processed using CellProfiler (Broad Institute, Cambridge, USA), and cells were classified and counted using the Advanced Cell Classifier. Synergistic drug effects were calculated using SynergyFinder tool (Yadav *et al*, 2015; Ianevski *et al*, 2020). Zero interaction potency scores (Z-scores) equal or greater than zero indicate additivity or synergism whereas Z-scores below zero demonstrate antagonism of 3d2 and Dexamethasone.

BiFC assay

Interaction of the GR and LRH-1 visualized by BiFC was analyzed by conventional and confocal fluorescence microscopy or flow cytometric analysis of YFP positive (YFP+) cells. Briefly, HEK 293H (6-well format, 1 μg DNA in total) and Jurkat cells were co-transfected with YFP1- and YFP2-tagged GR and LRH-1 expression vectors at a ratio of 1:1. For fluorescence microscopy, transfected cells were pre-treated for 24 h with 20 μM 3d2 or 5 μM SR1848 followed by treatment with 500 nM dexamethasone for 2 h. DMSO was used as solvent control. For nuclear counterstain, cells were incubated with Hoechst 33342 (1 μg/μl) for 20 min at room temperature (RT) and directly afterwards analyzed using either the epifluorescence microscope Zeiss Axio Observer Z1 (Carl Zeiss Microscopy, Oberkochen, Germany; filter set 44: excitation filter BP 475/40, beam splitter FT 500; emission filter BP 530/50) or the confocal microscope Zeiss LSM 880 equipped with an AiryScan detector (Carl Zeiss Microscopy; 514 nm argon laser for excitation, FITC filters/channel). Microscopy images taken with AxioVision or ZEN Software (Carl Zeiss Microscopy) were processed using ImageJ (National Institute of Health). For flow cytometric quantification of BiFC positive HEK 293H cells, cells were pre-treated with 20 μM 3d2 or 5 μM SR1848 for 6 h, before overnight incubation with 500 nM dexamethasone or DMSO as solvent control whereas Jurkat cells were treated for 2, 4 and 6 h with 10 μM dexamethasone. Cells were harvested and resuspended in PBS supplemented with 2% bovine serum albumin (BSA) and 2 mM EDTA. Flow cytometry was performed using the LSR Fortessa (BD Biosciences) and the FACS Diva Software (BD Biosciences). Data were analyzed using FlowJo software (FlowJo LLC).

Co-localization of GR and LRH-1

HEK 293T cells were co-transfected with 2 μg expression vectors encoding for eGFP-tagged hLRH-1 (pEGFP-hLRH-1a) as well as dsRed-tagged hGR (hGR-Red2), and 5×10^4 cells were re-seeded on coverslips one day after (24 well plate). After 24 h, cells were treated with 500 nM dexamethasone for 90 min, before fixation using acetone and subsequently covered with DAPI-containing mounting medium (Sigma-Aldrich). Samples were analyzed using the Axio Observer with a 20x objective and the following filter sets: eGFP (LRH-1)—44; dsRed (GR)—15; DAPI (nuclei)—49 and images were taken and merged using AxioVision Software. Microscopy images were processed using ImageJ.

Co-precipitation of GR and LRH-1

HEK 293T grown in 10 cm dishes (2.2×10^6 cells) were transiently transfected with 2 μg expression vectors coding for mh-GR, eGFP-LRH-1 and/or empty backbone vectors to adjust the total DNA

content. After 24 h, cells were either treated with 500 nM dexamethasone or DMSO as solvent control for 90 min. Transiently transfected cells were harvested, washed with PBS and incubated for 10 min at RT in 400 µl cytoplasmic protein extraction buffer (10 mM HEPES, 10 mM KCl, 1 mM DTT, 1% NP-40, protease inhibitor, in H_2O; pH 7). After 4 min full speed centrifugation, supernatants containing cytoplasmic extracts were harvested and the remaining cellular nuclei were lysed with 400 µl of nucleoplasmic protein extraction buffer (20 mM HEPES, 500 mM NaCl, 1 mM DTT, 10% glycerol, protease inhibitor, in H_2O) for 30 min at 4°C on a shaker (1,400 rpm). Nuclear lysates were cleared by centrifugation (14,000 *g*, 10 min, 4°C), before 100 µl of cyto- and nucleoplasmic supernatants were incubated with PBS-washed Ni^{2+} sepharose beads (GE Healthcare, Chicago, USA) for 30 min on a rotating wheel at RT for binding of the His-tagged GR. After 10 washing steps (1% Tween, 1 mM imidazole in PBS), 60 µl of 500 mM imidazole in PBS was added for 15 min at RT resulting in the release of His-tagged GR and its interaction partners from the beads into the supernatant. Twenty-four microliter of these His-tag pulldown samples and 16 µl of nucleoplasmic and cytoplasmic supernatants (input samples) were subjected to SDS-PAGE and immunoblot analysis as described below.

Nuclear translocation of the GR

After 2 h treatment with either 10 µM (Jurkat, MOLT-4; CEM-C1) or 1 µM (CEM-C7) dexamethasone (Dexa), cytoplasmatic and nuclear lysates of 2×10^6 T-ALL cells were prepared (see Co-Precipitation of GR and LRH-1). Samples were subsequently subjected to standard immunoblot analysis. Antibodies for PARP and Tubulin were used as nuclear and cytoplasmatic loading controls, respectively.

Luciferase reporter assay

HEK 293T (6-well plate format), MOLT-4 and Jurkat cells were transiently transfected with reporter plasmids encoding for a luciferase gene expressed under the control of the GC response element (GRE) or five copies of the LRH-1 response element (5xRE), as well as Myc/6xHis-tagged human GR and/or LRH-1, as indicated. Plasmids were normally used in 1:1 ratios, if not stated otherwise in the figure legend. Corresponding amounts of empty vectors (pGL3, pcDNA3.1) were transfected as negative controls and co-transfection with the bGal expression vector served as an internal transfection control (1/10 of total protein amount). One day after transfection, HEK 293T cells were re-seeded to 96-well flat-bottom plates (1.6×10^4 cells/well) and after 6 h either pre-treated with 1 µM of the GR antagonist RU486 (1 h) or directly treated with 500 nM dexamethasone, 20 µM 3d2 and/or 5 µM SR1848. Similarly, T-ALL reporter cells were treated with 5 nM (CEM-C7) or 10 µM dexamethasone (Jurkat, MOLT-4) and/or 40 µM 3d2 24 h after transfection. After overnight incubation, reporter cells were harvested by centrifugation and aspiration of the medium, and incubated with 100 µl lysis buffer (100 mM K_2HPO_4, 0.2% TritonX-100 in H_2O, pH 7.8) for 30–45 min on ice. Using a luminescent detecting plate reader (Infinite 200 PRO, Tecan), luciferase activity was assessed by addition of 50 µl adenosine 5′-triphosphate (ATP) solution (10 mM ATP, 20 mM $MgCl_2$, 35 mM Glycyl-glycine in H_2O) as well as 50 µl luciferin solution (270 µM Coenzyme-A, 470 µM luciferin, 20 mM $MgCl_2$, 35 mM Glycyl-glycine in H_2O) and bGal activity by adding the 105 µl of the substrate o-nitrophenyl-β-D-galactopyranoside (ONPG; 0.2 mg/ml ONPG, 60 mM Na_2HPO_4*$2H_2O$, 40 mM NaH_2PO_4*H_2O, 10 mM KCl, 1 mM $MgSO_4$*$7H_2O$, 50 mM 2-mercaptoethanol in H_2O) to 30 µl lysate/sample. Luminescence was calculated as relative light units (R.L.U.) by normalizing light units obtained from luciferase assays by the OD_{405nm} values obtained from the bGal assay.

Cell count-based proliferation assay

Wild type, stable LRH-1 and control knockdown T-ALL cells were seeded at a density of 5×10^4 cells/ml. Wild type T-ALL cells were directly treated with 3 µM dexamethasone, 20 µm 3d2, 1 µM SR1848 (CEM-C1, MOLT-4) or 4 µM SR1848 (Jurkat). Corresponding amounts of DMSO was added as solvent control. Every 24 h, the concentration of cells was monitored using a Neubauer hemocytometer.

Flow cytometric analysis of apoptosis and cell cycle

One day prior to experiments, an appropriate number of T-ALL cells was washed once with PBS and cells were seeded at a density of 3×10^5 viable cells/ml. After seeding 2.5–5 $\times 10^4$ cells per well of 96-well plates, T-ALL cells were exposed to the indicated amounts of 3d2, Cpd2, SR1848 and/or dexamethasone for 24, 48 or 72 h (V_{Final} = 200 µl), and subsequently harvested by centrifugation. For detection of apoptotic cell death, cells were resuspended in 200 µl AnnexinV binding buffer (10 mM HEPES, 150 mM NaCl, 5 mM KCl, 1 mM $MgCl_2$, 1.8 mM $CaCl_2$) containing fluorescein isothiocyanate (FITC)-labeled AnnexinV and stained for 10 min at 4°C. For simple cell cycle analysis as previously described by Nicoletti *et al* (1991), cells were permeabilized and stained (20 min, 4°C) with 100–200 µl hypotonic propidium iodide (PI) solution (10 µg/ml PI, 0.1% TritonX-100 in 0.5x PBS). To simultaneously analyze bidimensional cell cycle distribution (EdU-Alexa647 and DAPI) and apoptosis (AnnexinV+), cells were stained using the 647 EdU Click Proliferation Kit (BD Bioscience, San Jose, USA) according to the manufacturers' protocol. Flow cytometry was performed using the LSR Fortessa and the FACS Diva Software and 10,000 single cells were recorded for both apoptosis and cell cycle analysis. Flow cytometric data were analyzed using FlowJo software. Gating strategy for simultaneous flow cytometric analysis of cell cycle distribution by EdU/DAPI staining and cell death by AnnexinV staining: Sideward (SSC) and forward (FSC) scatter blots were used to gate cellular events and subsequently perform doublet discrimination. AnnexinV histograms were used to determine the number of apoptotic cells as a percentage of total cells. Contour blots were used to assess the cell cycle distribution of AnnexinV negative (AnnexinV−) viable cells based on EdU incorporation and DNA content (DAPI staining). Synergistic apoptosis induction by 3d2 and dexamethasone was calculated using SynergyFinder tool. The resulting mean, respectively, maximal ZIP score indicates synergy (ZIP score ≥1), additivity (ZIP score 0–1) or antagonism (ZIP score ≤0; Yadav *et al*, 2015; Ianevski *et al*, 2020).

RNA extraction and quantitative real-time PCR (qPCR)

For standard qPCR, approximately 2×10^6 T-ALL cells were lysed using either 1 ml peqGOLD TriFast TriFast™ (VWR, Darmstadt, Germany) or RNA-Solv® (Omega Bio-Tek, Norcross, USA), and RNA was isolated according to the manufacturers' protocols. After DNase I digest (New England Biolabs), a High-Capacity cDNA Reverse Transcription Kit (Applied Biosystems, Foster City, USA) was used to reverse transcribe 1–2 µg RNA into complementary DNA (cDNA).

For probe-based qPCR samples were prepared using Volcano Cell 2G lysis buffer according to the manufacturers' protocol (myPOLS Biotec, Konstanz, Germany). For quantification of gene expression classic and probe-based qPCR was performed using either Fast SYBR® Green Master Mix (Applied Biosystems) or Volcano Cell 2G RT-PCR 2x Master Mix (myPOLS Biotec), in a StepOnePlus Real-time PCR system (Applied Biosystems). Transcript levels were normalized to beta-Actin (β-Actin) and depicted as $2^{-\Delta Ct}$ ($\Delta C_t = C_t$ target gene $- C_t$ β-Actin gene) or presented as fold change to corresponding controls. All qPCR primer and probe sequences used in this study are listed in Table EV2.

Immunoblot analysis

For immunoblot analysis, roughly 1–2 × 10^6 T-ALL cells were seeded per well of 6-well plates at a density of 2–3 × 10^5 cells/ml. After treatment as indicated in the corresponding figure legends, T-ALL cells were harvested by centrifugation and washed once with ice-cold PBS before being lysed using RIPA buffer (radioimmunoprecipitation assay buffer; 50 mM Tris, 150 mM NaCl, 0.1% SDS, 0.5% sodium deoxycholate, 1% NP40 in H_2O, pH 7.8). Equal amounts of protein (15–25 μg) were loaded on 12% SDS-PAGE, electrophoretically separated by size and subsequently transferred onto polyvinylidene difluoride membranes (Roche Diagnostics, Mannheim, Germany). After overnight incubation at 4°C with primary antibodies, membranes were incubated for 1 h with corresponding horse radish-coupled secondary antibodies and ECL developing reagent (2.5 mM Luminol, 0.4 mM p-Coumaric acid, 10 mM Tris, 0.015% H_2O_2 in H_2O, pH 8.5) was added for imaging using an Image Quant LAS 4000 (GE Healthcare) for detection of chemiluminescent signal. PARP, GR, Myc, Cyclin E1, phospho-AMPK, phospho-p38, cleaved caspase 3, Bim and Bcl-2 antibodies were purchased from Cell Signaling Technology (Danvers, USA). Antibody for detection of GFP was ordered from Roche and for full-length Caspase 3 from Calbiochem (Darmstadt, Germany). The antibody for Tubulin, which was used as loading control, was obtained from Sigma-Aldrich.

Quantification and statistical analysis

For all figures, data are presented as mean ± SD of technical or experimental replicates as indicated in the figure legends. "n" represents the number of independent experiments performed. Significant differences were calculated using either paired or unpaired t-test, one-way or two-way ANOVA using Prism 8 (Graphpad Software). Differences were considered as significant for P values of $^*P < 0.05$; $^{**}P < 0.01$; $^{***}P < 0.001$. Statistical details for individual experiments are specified in the corresponding figure legends. Prism 8 was also used to perform linear regression and calculate Pearson's correlation coefficients shown in Fig 7D.

Data availability

This study includes no data deposited in external repositories.

Expanded View for this article is available online.

Acknowledgements

We thank Thomas U. Mayer and Thomas Böttcher for helpful discussions and advice, Daniel Legler for providing BiFC constructs, Verena Merk and Ann-Kristin Hildebrand for expert technical help. The study was supported by the DFG-funded Konstanz Research School-Chemical Biology (KoRS-CB, GSC 2018) and the Swiss Cancer League (to Beat Bornhauser, KFS-4384-02-2018) and S.M. received a fellowship from the Carl Zeiss Foundation. The schematic summary figure was created with BioRender.com. Open Access funding enabled and organized by Projekt DEAL.

Author contributions

Svenja Michalek: Formal analysis; investigation; writing – original draft. **Thomas Goj:** Formal analysis; investigation. **Anna Pia Plazzo:** Visualization. **Blerim Marovca:** Formal analysis; investigation. **Beat Bornhauser:** Conceptualization; supervision. **Thomas Brunner:** Conceptualization; supervision; funding acquisition; writing – original draft; project administration; writing – review and editing.

In addition to the CRediT author contributions listed above, the contributions in detail are:

TB and SM and designed the project and experiments; BB and TB supervised the project; SM, TG and BM conducted experiments; APP developed cloning strategy; SM analyzed, validated and visualized the data; SM and TB wrote the manuscript.

Disclosure and competing interests statement

The authors declare that they have no conflict of interest.

References

Almawi WY, Melemedjian OK (2002) Molecular mechanisms of glucocorticoid antiproliferative effects: antagonism of transcription factor activity by glucocorticoid receptor. *J Leukoc Biol* 71: 9 – 15

Amoutzias GD, Pichler EE, Mian N, De Graaf D, Imsiridou A, Robinson-Rechavi M, Bornberg-Bauer E, Robertson DL, Oliver SG (2007) A protein interaction atlas for the nuclear receptors: properties and quality of a hub-based dimerisation network. *BMC Syst Biol* 1: 34

Bachmann PS, Gorman R, Papa RA, Bardell JE, Ford J, Kees UR, Marshall GM, Lock RB (2007) Divergent mechanisms of glucocorticoid resistance in experimental models of pediatric acute lymphoblastic leukemia. *Cancer Res* 67: 4482 – 4490

Bayrer JR, Wang H, Nattiv R, Suzawa M, Escusa HS, Fletterick RJ, Klein OD, Moore DD, Ingraham HA (2018) LRH-1 mitigates intestinal inflammatory disease by maintaining epithelial homeostasis and cell survival. *Nat Commun* 9: 4055

Beck CA, Estes PA, Bona BJ, Muro-Cacho CA, Nordeen SK, Edwards DP (1993) The steroid antagonist RU486 exerts different effects on the glucocorticoid and progesterone receptors. *Endocrinology* 133: 728 – 740

Benod C, Carlsson J, Uthayaruban R, Hwang P, Irwin JJ, Doak AK, Shoichet BK, Sablin EP, Fletterick RJ (2013) Structure-based discovery of antagonists of nuclear receptor LRH-1. *J Biol Chem* 288: 19830 – 19844

Bookout AL, Jeong Y, Downes M, Yu RT, Evans RM, Mangelsdorf DJ (2006) Anatomical profiling of nuclear receptor expression reveals a hierarchical transcriptional network. *Cell* 126: 789 – 799

Bornhauser BC, Bonapace L, Lindholm D, Martinez R, Cario G, Schrappe M, Niggli FK, Schäfer BW, Bourquin J-P (2007) Low-dose arsenic trioxide sensitizes glucocorticoid-resistant acute lymphoblastic leukemia cells to dexamethasone via an Akt-dependent pathway. *Blood* 110: 2084 – 2091

de Bosscher K, vanden Berghe W, Haegeman G (2003) The interplay between the glucocorticoid receptor and nuclear factor-κB or activator protein-1: molecular mechanisms for gene repression. *Endocr Rev* 24: 488 – 522

Botrugno OA, Fayard E, Annicotte JS, Haby C, Brennan T, Wendling O, Tanaka T, Kodama T, Thomas W, Auwerx J *et al* (2004) Synergy between LRH-1 and beta-catenin induces G1 cyclin-mediated cell proliferation. *Mol Cell* 15: 499 – 509

Brown JA, Ferrando A (2018) Glucocorticoid resistance in acute lymphoblastic leukemia: BIM finally. *Cancer Cell* 34: 869 – 871

Brumatti G, Yon M, Castro FA, Bueno-da-Silva AEB, Jacysyn JF, Brunner T, Amarante-Mendes GP (2008) Conversion of CD95 (Fas) Type II into Type I signaling by sub-lethal doses of cycloheximide. *Exp Cell Res* 314: 554 – 563

Canovas B, Nebreda AR (2021) Diversity and versatility of p38 kinase signalling in health and disease. *Nat Rev Mol Cell Biol* 22: 346 – 366

Chen Q, Yuan H, Shi GD, Wu Y, Liu DF, Lin YT, Chen L, Ge WL, Jiang K, Miao Y (2018) Association between NR5A2 and the risk of pancreatic cancer, especially among Caucasians: a meta-analysis of case-control studies. *Onco Targets Ther* 11: 2709 – 2723

Clarisse D, Offner F, De Bosscher K (2020) Latest perspectives on glucocorticoid-induced apoptosis and resistance in lymphoid malignancies. *Biochim Biophys Acta Rev Cancer* 1874: 188430

Corzo CA, Mari Y, Chang MR, Khan T, Kuruvilla D, Nuhant P, Kumar N, West GM, Duckett DR, Roush WR *et al* (2015) Antiproliferation activity of a small molecule repressor of liver receptor homolog 1. *Mol Pharmacol* 87: 296 – 304

Crowley LC, Marfell BJ, Scott AP, Waterhouse NJ (2016) Quantitation of apoptosis and necrosis by annexin v binding, propidium iodide uptake, and flow cytometry. *Cold Spring Harb Protoc* 2016: pdb.prot087288

Elion EA (2006) Detection of protein-protein interactions by coprecipitation. *Curr Protoc Neurosci* 35: 5.25.21 – 25.25.10

Escoter-Torres L, Caratti G, Mechtidou A, Tuckermann J, Uhlenhaut NH, Vettorazzi S (2019) Fighting the fire: mechanisms of inflammatory gene regulation by the glucocorticoid receptor. *Front Immunol* 10: 1859

Frismantas V, Dobay MP, Rinaldi A, Tchinda J, Dunn SH, Kunz J, Richter-Pechanska P, Marovca B, Pail O, Jenni S *et al* (2017) *Ex vivo* drug response profiling detects recurrent sensitivity patterns in drug-resistant acute lymphoblastic leukemia. *Blood* 129: e26 – e37

Guo X, Zhou CY, Li Q, Gao J, Zhu YP, Gu L, Ma ZG (2013) Rapamycin sensitizes glucocorticoid resistant acute lymphoblastic leukemia CEM-C1 cells to dexamethasone induced apoptosis through both mTOR suppression and up-regulation and activation of glucocorticoid receptor. *Biomed Environ Sci* 26: 371 – 381

Hauser MA, Schaeuble K, Kindinger I, Impellizzieri D, Krueger WA, Hauck CR, Boyman O, Legler DF (2016) Inflammation-induced CCR7 oligomers form scaffolds to integrate distinct signaling pathways for efficient cell migration. *Immunity* 44: 59 – 72

Hefazi M, Litzow MR (2018) Recent advances in the biology and treatment of T cell acute lymphoblastic leukemia. *Curr Hematol Malig Rep* 13: 265 – 274

Heidari N, Miller AV, Hicks MA, Marking CB, Harada H (2012) Glucocorticoid-mediated BIM induction and apoptosis are regulated by Runx2 and c-Jun in leukemia cells. *Cell Death Dis* 3: e349

Heng JC, Feng B, Han J, Jiang J, Kraus P, Ng JH, Orlov YL, Huss M, Yang L, Lufkin T *et al* (2010) The nuclear receptor Nr5a2 can replace Oct4 in the reprogramming of murine somatic cells to pluripotent cells. *Cell Stem Cell* 6: 167 – 174

Herold MJ, McPherson KG, Reichardt HM (2006) Glucocorticoids in T cell apoptosis and function. *Cell Mol Life Sci* 63: 60 – 72

Hodgens A, Sharman T (2022) Corticosteroids. In *StatPearls*. Treasure Island, FL: StatPearls Publishing

Huang SC, Lee CT, Chung BC (2014) Tumor necrosis factor suppresses NR5A2 activity and intestinal glucocorticoid synthesis to sustain chronic colitis. *Sci Signal* 7: ra20

Hume S, Dianov GL, Ramadan K (2020) A unified model for the G1/S cell cycle transition. *Nucleic Acids Res* 48: 12483 – 12501

Ianevski A, Giri AK, Aittokallio T (2020) SynergyFinder 2.0: visual analytics of multi-drug combination synergies. *Nucleic Acids Res* 48: W488 – W493

Ianevski A, He L, Aittokallio T, Tang J (2017) SynergyFinder: a web application for analyzing drug combination dose-response matrix data. *Bioinformatics* 33: 2413 – 2415

Inaba H, Pui CH (2010) Glucocorticoid use in acute lymphoblastic leukaemia. *Lancet Oncol* 11: 1096 – 1106

Jing D, Bhadri VA, Beck D, Thoms JA, Yakob NA, Wong JW, Knezevic K, Pimanda JE, Lock RB (2015) Opposing regulation of BIM and BCL2 controls glucocorticoid-induced apoptosis of pediatric acute lymphoblastic leukemia cells. *Blood* 125: 273 – 283

Kerppola TK (2008) Bimolecular fluorescence complementation (BiFC) analysis as a probe of protein interactions in living cells. *Annu Rev Biophys* 37: 465 – 487

Kingston RE, Chen CA, Rose JK (2003) Calcium phosphate transfection. *Curr Protoc Mol Biol* 63: 9.1.1 – 9.1.11

Kininis M, Kraus WL (2008) A global view of transcriptional regulation by nuclear receptors: gene expression, factor localization, and DNA sequence analysis. *Nucl Recept Signal* 6: e005

Lee Y-K, Schmidt DR, Cummins CL, Choi M, Peng L, Zhang Y, Goodwin B, Hammer RE, Mangelsdorf DJ, Kliewer SA (2008) liver receptor homolog-1 regulates bile acid homeostasis but is not essential for feedback regulation of bile acid synthesis. *Mol Endocrinol* 22: 1345 – 1356

Lefevre L, Authier H, Stein S, Majorel C, Couderc B, Dardenne C, Eddine MA, Meunier E, Bernad J, Valentin A *et al* (2015) LRH-1 mediates anti-inflammatory and antifungal phenotype of IL-13-activated macrophages through the PPARgamma ligand synthesis. *Nat Commun* 6: 6801

Liberman AC, Budziñski ML, Sokn C, Gobbini RP, Steininger A, Arzt E (2018) Regulatory and mechanistic actions of glucocorticoids on T and inflammatory cells. *Front Endocrinol* 9

Liden J, Delaunay F, Rafter I, Gustafsson J-Å, Okret S (1997) A new function for the C-terminal zinc finger of the glucocorticoid receptor: repression of RelA transactivation. *J Biol Chem* 272: 21467 – 21472

Liu Y, Ge J, Li Q, Guo X, Gu L, Ma Z-G, Li X-H, Zhu Y-P (2014) Low-dose anisomycin sensitizes glucocorticoid-resistant T-acute lymphoblastic leukemia CEM-C1 cells to dexamethasone-induced apoptosis through activation of glucocorticoid receptor and p38-MAPK/JNK. *Leuk Lymphoma* 55: 2179 – 2188

Liu L, Li Y, Pan B, Zhang T, Wei D, Zhu Y, Guo Y (2019) Nr5a2 promotes tumor growth and metastasis of gastric cancer AGS cells by Wnt/beta-catenin signaling. *Onco Targets Ther* 12: 2891 – 2902

Lopez-Royuela N, Balsas P, Galan-Malo P, Anel A, Marzo I, Naval J (2010) Bim is the key mediator of glucocorticoid-induced apoptosis and of its potentiation by rapamycin in human myeloma cells. *Biochim Biophys Acta* 1803: 311 – 322

Louw A (2019) GR dimerization and the impact of GR dimerization on GR protein stability and half-life. *Front Immunol* 10: 1693

Mamrosh JL, Lee JM, Wagner M, Stambrook PJ, Whitby RJ, Sifers RN, Wu SP, Tsai MJ, Demayo FJ, Moore DD (2014) Nuclear receptor LRH-1/NR5A2 is required and targetable for liver endoplasmic reticulum stress resolution. *elife* 3: e01694

Mangelsdorf DJ, Thummel C, Beato M, Herrlich P, Schutz G, Umesono K, Blumberg B, Kastner P, Mark M, Chambon P *et al* (1995) The nuclear receptor superfamily: the second decade. *Cell* 83: 835 – 839

Martens C, Bilodeau S, Maira M, Gauthier Y, Drouin J (2005) Protein-protein interactions and transcriptional antagonism between the subfamily of

NGFI-B/Nur77 orphan nuclear receptors and glucocorticoid receptor. *Mol Endocrinol* 19: 885 – 897

Mataki C, Magnier BC, Houten SM, Annicotte J-S, Argmann C, Thomas C, Overmars H, Kulik W, Metzger D, Auwerx J *et al* (2007) Compromised intestinal lipid absorption in mice with a liver-specific deficiency of liver receptor homolog 1. *Mol Cell Biol* 27: 8330 – 8339

McKay LI, Cidlowski JA (1998) Cross-talk between nuclear factor-kappa B and the steroid hormone receptors: mechanisms of mutual antagonism. *Mol Endocrinol* 12: 45 – 56

Merk VM, Phan TS, Brunner T (2021) Regulation of tissue immune responses by local glucocorticoids at epithelial barriers and their impact on interorgan crosstalk. *Front Immunol* 12

Michalek S, Brunner T (2020) Nuclear-mitochondrial crosstalk: on the role of the nuclear receptor liver receptor homolog-1 (NR5A2) in the regulation of mitochondrial metabolism, cell survival, and cancer. *IUBMB Life* 73: 592 – 610

Mihara K, Imai C, Coustan-Smith E, Dome JS, Dominici M, Vanin E, Campana D (2003) Development and functional characterization of human bone marrow mesenchymal cells immortalized by enforced expression of telomerase. *Br J Haematol* 120: 846 – 849

Misselwitz B, Strittmatter G, Periaswamy B, Schlumberger MC, Rout S, Horvath P, Kozak K, Hardt W-D (2010) Enhanced CellClassifier: a multi-class classification tool for microscopy images. *BMC Bioinformatics* 11: 30

Murphy B, Yin H, Maris JM, Kolb EA, Gorlick R, Reynolds CP, Kang MH, Keir ST, Kurmasheva RT, Dvorchik I *et al* (2016) Evaluation of alternative *in vivo* drug screening methodology: a single mouse analysis. *Cancer Res* 76: 5798 – 5809

Nadolny C, Dong X (2015) Liver receptor homolog-1 (LRH-1): a potential therapeutic target for cancer. *Cancer Biol Ther* 16: 997 – 1004

Nicolaides NC, Pavlaki AN, Maria Alexandra MA, Chrousos GP (2000) Glucocorticoid therapy and adrenal suppression. In *Endotext*, KR Feingold, B Anawalt, A Boyce, G Chrousos, K Dungan, A Grossman, JM Hershman, G Kaltsas, C Kosh, P Kopp *et al* (eds). South Dartmouth, MA: MDText.com, Inc

Nicoletti I, Migliorati G, Pagliacci MC, Grignani F, Riccardi C (1991) A rapid and simple method for measuring thymocyte apoptosis by propidium iodide staining and flow cytometry. *J Immunol Methods* 139: 271 – 279

Nyfeler B, Michnick SW, Hauri HP (2005) Capturing protein interactions in the secretory pathway of living cells. *Proc Natl Acad Sci U S A* 102: 6350 – 6355

O'Connor L, Strasser A, O'Reilly LA, Hausmann G, Adams JM, Cory S, Huang DC (1998) Bim: a novel member of the Bcl-2 family that promotes apoptosis. *EMBO J* 17: 384 – 395

Olivas-Aguirre M, Torres-López L, Pottosin I, Dobrovinskaya O (2021) Overcoming glucocorticoid resistance in acute lymphoblastic leukemia: repurposed drugs can improve the protocol. *Front Oncol* 11: 647

Oosterveer MH, Mataki C, Yamamoto H, Harach T, Moullan N, van Dijk TH, Ayuso E, Bosch F, Postic C, Groen AK *et al* (2012) LRH-1-dependent glucose sensing determines intermediary metabolism in liver. *J Clin Invest* 122: 2817 – 2826

Ortlund EA, Lee Y, Solomon IH, Hager JM, Safi R, Choi Y, Guan Z, Tripathy A, Raetz CR, McDonnell DP *et al* (2005) Modulation of human nuclear receptor LRH-1 activity by phospholipids and SHP. *Nat Struct Mol Biol* 12: 357 – 363

Pang JB, Molania R, Chand A, Knower K, Takano EA, Byrne DJ, Mikeska T, Millar EKA, Lee CS, O'Toole SA *et al* (2017) LRH-1 expression patterns in breast cancer tissues are associated with tumour aggressiveness. *Oncotarget* 8: 83626 – 83636

Pare JF, Malenfant D, Courtemanche C, Jacob-Wagner M, Roy S, Allard D, Belanger L (2004) The fetoprotein transcription factor (FTF) gene is essential to embryogenesis and cholesterol homeostasis and is regulated by a DR4 element. *J Biol Chem* 279: 21206 – 21216

Pearson OH, Eliel LP (1950) Use of pituitary adrenocorticotropic hormone (ACTH) and cortisone in lymphomas and leukemias. *J Am Med Assoc* 144: 1349 – 1353

Petrillo M, Bortner C, Cidlowski J (2017) Glucocorticoids: Inflammation and immunity. In *The hypothalamic-pituitary-adrenal axis in health and disease*, AB Geer (ed) pp 43 – 63. Cham: Springer International Publishing

Picard D, Yamamoto KR (1987) Two signals mediate hormone-dependent nuclear localization of the glucocorticoid receptor. *EMBO J* 6: 3333 – 3340

Porter BA, Ortiz MA, Bratslavsky G, Kotula L (2019) Structure and function of the nuclear receptor superfamily and current targeted therapies of prostate cancer. *Cancer* 11: 1852

Ramdas J, Liu W, Harmon JM (1999) Glucocorticoid-induced cell death requires autoinduction of glucocorticoid receptor expression in human leukemic T cells. *Cancer Res* 59: 1378 – 1385

Richter-Pechańska P, Kunz JB, Bornhauser B, von Knebel DC, Rausch T, Erarslan-Uysal B, Assenov Y, Frismantas V, Marovca B, Waszak SM *et al* (2018) PDX models recapitulate the genetic and epigenetic landscape of pediatric T-cell leukemia. *EMBO Mol Med* 10

Riml S, Schmidt S, Ausserlechner MJ, Geley S, Kofler R (2004) Glucocorticoid receptor heterozygosity combined with lack of receptor auto-induction causes glucocorticoid resistance in Jurkat acute lymphoblastic leukemia cells. *Cell Death Differ* 11: S65 – S72

Sablin EP, Krylova IN, Fletterick RJ, Ingraham HA (2003) Structural basis for ligand-independent activation of the orphan nuclear receptor LRH-1. *Mol Cell* 11: 1575 – 1585

Sanjana NE, Shalem O, Zhang F (2014) Improved vectors and genome-wide libraries for CRISPR screening. *Nat Methods* 11: 783 – 784

Saraste A, Pulkki K (2000) Morphologic and biochemical hallmarks of apoptosis. *Cardiovasc Res* 45: 528 – 537

Schmitz M, Breithaupt P, Scheidegger N, Cario G, Bonapace L, Meissner B, Mirkowska P, Tchinda J, Niggli FK, Stanulla M *et al* (2011) Xenografts of highly resistant leukemia recapitulate the clonal composition of the leukemogenic compartment. *Blood* 118: 1854 – 1864

Schoonjans K, Annicotte JS, Huby T, Botrugno OA, Fayard E, Ueda Y, Chapman J, Auwerx J (2002) Liver receptor homolog 1 controls the expression of the scavenger receptor class B type I. *EMBO Rep* 3: 1181 – 1187

Schule R, Rangarajan P, Kliewer S, Ransone LJ, Bolado J, Yang N, Verma IM, Evans RM (1990) Functional antagonism between oncoprotein c-Jun and the glucocorticoid receptor. *Cell* 62: 1217 – 1226

Schwaderer J, Gaiser A-K, Phan TS, Delgado M, Brunner T (2017) Liver receptor homolog-1 (NR5a2) regulates CD95/Fas ligand transcription and associated T-cell effector functions. *Cell Death Dis* 8: e2745

Schwaderer J, Phan TS, Glockner A, Delp J, Leist M, Brunner T, Delgado ME (2020) Pharmacological LRH-1/Nr5a2 inhibition limits pro-inflammatory cytokine production in macrophages and associated experimental hepatitis. *Cell Death Dis* 11: 154

Seitz C, Huang J, Geiselhoringer AL, Galbani-Bianchi P, Michalek S, Phan TS, Reinhold C, Dietrich L, Schmidt C, Corazza N *et al* (2019) The orphan nuclear receptor LRH-1/NR5a2 critically regulates T cell functions. *Sci Adv* 5: eaav9732

Sionov RV, Vlahopoulos SA, Granot Z (2015) Regulation of bim in health and disease. *Oncotarget* 6: 23058 – 23134

Smith LK, Cidlowski JA (2010) Glucocorticoid-induced apoptosis of healthy and malignant lymphocytes. *Prog Brain Res* 182: 1 – 30

Stein S, Schoonjans K (2015) Molecular basis for the regulation of the nuclear receptor LRH-1. *Curr Opin Cell Biol* 33: 26 – 34

Terwilliger T, Abdul-Hay M (2017) Acute lymphoblastic leukemia: a comprehensive review and 2017 update. *Blood Cancer J* 7: e577

Timmermans S, Souffriau J, Libert C (2019) A general introduction to glucocorticoid biology. *Front Immunol* 10: 1545

Uhlén M, Fagerberg L, Hallström BM, Lindskog C, Oksvold P, Mardinoglu A, Sivertsson Å, Kampf C, Sjöstedt E, Asplund A *et al* (2015) Proteomics. Tissue-based map of the human proteome. *Science* 347: 1260419

Weikum ER, Liu X, Ortlund EA (2018) The nuclear receptor superfamily: a structural perspective. *Protein Sci* 27: 1876 – 1892

Wu C, Feng J, Li L, Wu Y, Xie H, Yin Y, Ye J, Li Z (2018) Liver receptor homologue 1, a novel prognostic marker in colon cancer patients. *Oncol Lett* 16: 2833 – 2838

Xiao L, Wang Y, Liang W, Liu L, Pan N, Deng H, Li L, Zou C, Chan FL, Zhou Y (2018) LRH-1 drives hepatocellular carcinoma partially through induction of c-myc and cyclin E1, and suppression of p21. *Cancer Manag Res* 10: 2389 – 2400

Xu P, Oosterveer MH, Stein S, Demagny H, Ryu D, Moullan N, Wang X, Can E, Zamboni N, Comment A *et al* (2016) LRH-1-dependent programming of mitochondrial glutamine processing drives liver cancer. *Genes Dev* 30: 1255 – 1260

Yadav B, Wennerberg K, Aittokallio T, Tang J (2015) Searching for Drug Synergy in Complex Dose-Response Landscapes Using an Interaction Potency Model. *Comput Struct Biotechnol J* 13: 504 – 513